3-10-2010

Optical and Electrical Characterization of Bulk Grown Indium-Gallium-Arsenide Alloys

Austin C. Bergstrom

OPTICAL AND ELECTRICAL CHARACTERIZATION OF BULK GROWN INDIUM-GALLIUM-ARSENIDE ALLOYS

THESIS

Austin C. Bergstrom, 2nd Lieutenant, USAF

AFIT/GAP/ENP/10-M02

DEPARTMENT OF THE AIR FORCE
AIR UNIVERSITY

AIR FORCE INSTITUTE OF TECHNOLOGY

Wright-Patterson Air Force Base, Ohio

The views expressed in this thesis are those of the author and do not reflect the official policy or position of the United States Air Force, Department of Defense, or the U.S. Government.

AFIT/GAP/ENP/10-M02

OPTICAL AND ELECTRICAL CHARACTERIZATION OF BULK GROWN INDIUM-GALLIUM-ARSENIDE ALLOYS

THESIS

Presented to the Faculty

Department of Engineering Physics

Graduate School of Engineering and Management

Air Force Institute of Technology

Air University

Air Education and Training Command

In Partial Fulfillment of the Requirements for the

Degree of Master of Science in Engineering Physics

Austin C. Bergstrom, BS

2nd Lieutenant, USAF

March 2010

AFIT/GAP/ENP/10-M02

OPTICAL AND ELECTRICAL CHARACTERIZATION OF BULK GROWN INDIUM-GALLIUM-ARSENIDE ALLOYS

Austin C Bergstrom, BS

2nd Lieutenant, USAF

Approved:

Yung Kee Yeo, PhD (Chairman)	Date
Robert Hengehold, PhD (Member)	Date
Alex Li, PhD (Member)	Date

Abstract

Advances in crystal growth techniques have allowed increased quality in growth of bulk ternary $In_xGa_{1-x}As$. Here, the optical and electrical properties of samples grown through the vertical Bridgman (or multi-component zone melting growth) method have been investigated through photoluminescence spectroscopy and Hall effect measurements. Indium mole fractions varied from 0.75 for 1. Hall effect measurements at temperatures ranging from 10 to 300 K revealed moderate n-type doping with carrier concentrations ranging from 1.5 to 9.6×10^{16} cm^{-3} at 10 to 15 K. Carriers from deep donor levels became appreciable between 50 and 100 K. Hall mobility increased with rising indium content, and mobility values at 15 K ranged from 1.5×10^{4} $cm^2/(V\cdot s)$ for $In_{0.75}Ga_{0.25}As$ to 3.5×10^{4} $cm^2/(V\cdot s)$ for InAs. Mobility variation with temperature showed ionized impurity scattering to be dominant at low temperatures with optical phonon scattering becoming dominant near 100 K. Laser excitation power dependent photoluminescence measurements were performed at 12 K, and temperature dependent photoluminescence measurements were performed at temperatures ranging from approximately 12 to 140 K. Photoluminescence measurements showed band-to-band and donor-acceptor pair transitions. 12 K band-to-band photoluminescence peak positions loosely followed predicted band gaps, and position dependent photoluminescence measurements revealed varying degrees of uniformity across the samples studied.

Acknowledgments

Dr. Yung Kee Yeo, my advisor, deserves many thanks for all of his advice and insights throughout the project. His assistance was indispensible. Mike Ranft and Greg Smith were both absolutely invaluable. They offered countless tips on the minutiae of lab equipment, provided trouble shooting help, and set things straight when I came perilously near to serious damage. Without them the project would probably still be stuck around week three. Travis Gomez was also of great assistance, particularly early on, as I learned the various systems I would be using, generously giving up his time to help me continue research that he was instrumental in starting. Dr. Alex Li and Dr. Robert Hengehold gave very useful feedback as my thesis neared completion, particularly in drawing conclusions and suggesting future research. Thanks also to Doug Macdonald, who offered some very helpful MATLAB code for uploading text files with ill-behaved headers, Jean Wei, who provided absorption data and countless pieces of background information on the samples studied, Matthew Spidell, who gave me a homemade preamplifier he had built when the original preamplifier used on the photoluminescence measurements failed, and all who read my draft for typos and grammatical errors.

Austin Bergstrom

Table of Contents

Page

List of Figures

Figure Page

Figure Page

Figure Page

List of Tables

Table Page

OPTICAL AND ELECTRICAL CHARACTERIZATION OF BULK GROWN INDIUM-GALLIUM-ARSENIDE ALLOYS

I. Introduction

Background

A variety of semiconductor devices including field effect transistors, lasers, and photodetectors have traditionally been fabricated through growth of epitaxial layers on binary or elemental substrates, but limitations in buffer layer technologies connecting binary substrates (which offer a discrete set of available lattice constants) to device layers have hampered performance [1]. Large, single-crystal substrates consisting of ternary alloys with tunable lattice constants and band gaps solve this problem and allow possibilities for a host of new epitaxial IR devices [1, 2]. Device quality substrates, however, have proven elusive to develop because of difficulties associated with growing them from melts, largely due to the challenge of maintaining uniform composition [1-4]. In his 2005 review of bulk ternary III-V substrate growth [1], P.S. Dutta listed five requirements of these alloys for achieving broad applicability, namely: "(a) spatial compositional homogeneity better than 0.5 mol% across the wafer, (b) extremely low defect content (no inclusions or multi-phase regions, crack free, dislocation density less than 100 cm^{-2}), (c) tunable optical and electrical properties, (d) low built-in strain in the crystals enabling wafer slicing and polishing and (e) cost of final wafers not significantly higher than commercially available binary substrates." It is against this rubric that bulk ternary crystals are evaluated for their prospects in device applications.

The $In_xGa_{1-x}As$ samples analyzed here were grown using the vertical Bridgman or multi-component zone melting growth method (MCZM) by the United Semiconductors LLC. The MCZM growth process (outlined nicely by Nishijima [5]) starts with a ternary seed crystal gown via the vertical gradient freeze (VGF) method on a GaAs substrate. The VGF crystal has varying composition in which the In content usually increases monotonically from the GaAs seed to the growth interface, at which point the seed crystal has the desired In content for final crystal. A ternary $In_xGa_{1-x}As$ seed crystal produced by rapid freezing of an $In_xGa_{1-x}As$ melt of the desired composition is used as the source material for the final MCZM crystal. The $In_xGa_{1-x}As$ seed crystal and its GaAs substrate are placed atop a heat sink, and these are placed beneath the ternary $In_xGa_{1-x}As$ source within a quartz ampule inside of a furnace. The furnace is raised to the growth temperature of the crystal, and the ternary $In_xGa_{1-x}As$ source is gradually fused to the $In_xGa_{1-x}As$ seed crystal. MCZM maintains the desired crystal composition by slowly moving the growing crystal toward to lower temperature end of the furnace in order to keep the growth interface at the correct position along the furnace's temperature profile, ultimately producing a crystal of uniform composition which can be cut from the seed VGF crystal. More detail on the growth method can be found in references 1 and 5-9.

Objectives

The objective of this research is to characterize $In_xGa_{1-x}As$ samples grown using the MCZM and provide an assessment of progress toward reaching device quality. This characterization will employ photoluminescence (PL) measurements to assess band gap energy, donor/acceptor levels, and impurity content as well as Hall Effect measurements

to determine carrier concentrations and mobility. These measurements provide data on fundamental material parameters and offer an understanding of the progress toward the growth of device-quality crystals.

Semiconductor Basics

The following provides a cursory overview of some of the more basic concepts helpful in understanding semiconductors. It is designed primarily to explain some of the more critical definitions unique to solid state physics used later on in this study.

An ideal semiconductor at absolute zero has a completely full valence band and a completely empty conduction band, where the bands consist of a set of electronic quantum states and their corresponding energies. In a semiconductor, the valence band is separated from the conduction band by the band gap, an energy range for which there are no allowed quantum states in the crystal. This energy separation is of greatest importance because neither a completely full band (one in which every electronic state is occupied) nor a completely empty band can carry a current. In essence, with all electronic states occupied, there can be no net change in the quantum states of the band and hence no net charge movement. Heuristically, it is similar to a completely full parking lot; empty spots are required for cars to move about.

The conduction band may gain charge carriers when electrons are excited from the valence band, perhaps thermally or by photons above band gap energy, and from impurities known as donors which create electronic energy states very near to the conduction band's low energy edge. Electrons in these donor levels (generally a few meV below the band edge) are easily excited to the conduction band even at low

temperatures and generally "freeze out" between liquid nitrogen and liquid helium temperatures. In addition to processes promoting electrons from the valence to the conduction band, the valence band may lose elections to acceptor impurities. Acceptors create electronic energy states just above the band edge, generally at a slightly greater energy separation from the valence band edge than the separation of donors from the conduction band edge. These vacancies in the valence band, known as holes, allow the band to carry current as electrons transition to unoccupied states. These holes can be considered positive charge carriers, analogous to the convention holding that current is the flow of positive charge when in fact it is negatively charged electrons drifting the opposite direction of the current vector. This net motion of electrons in the valence band can be fully modeled by the motion of these positively charged holes, or empty electronic quantum states.

These relatively basic concepts relating to charge carriers, their origins, and the implications of impurities constitute the basis for much of the work presented in this study.

Optical Characterization Theory

Photoluminescence (PL) spectroscopy uses photons above band gap energy to excite electrons from the valence band and measure the radiative relaxation that occurs. Figure 1 below shows the various radiative relaxations that these electrons can undergo.

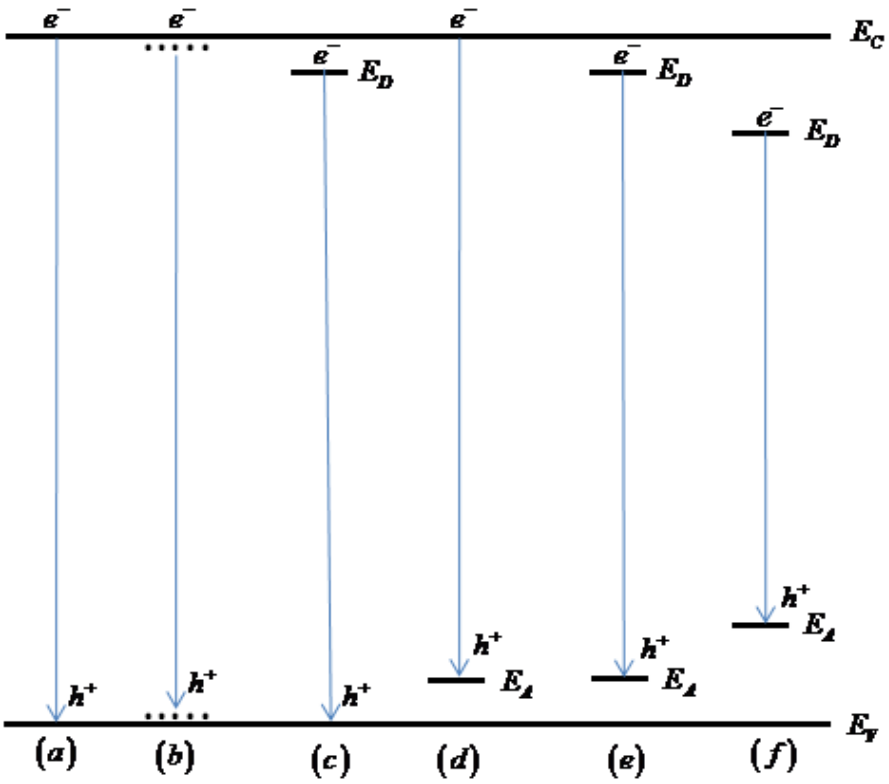

Figure 1. Schematic diagram of band edge photoluminescence emission. The types of light-emitting transitions depicted are (a) band-to-band, (b) free exciton, (c) neutral donor to free hole, (d) free electron to neutral acceptor (e) shallow donor-acceptor pair, and (f) deep state donor-acceptor pair [10]

Electrons excited to the conduction band decay through phonon coupling to a thermal distribution at the bottom of the conduction band on extremely short timescales (as little as 100 fs). Once electrons have decayed to the low-lying energy states in their respective bands, the electrons and holes exhibit behavior of quasi-equilibrium and each species establishes a unique Fermi energy depending upon its distribution and density. In the limits of low carrier density, the carriers equilibrate to the classical Boltzmann distribution, and band-to-band PL emission spectrum rises sharply at the band gap energy and then falls off with an exponential decay constant of kT [11]. In the case of high

carrier density (generally due to a high impurity content), Fermi-Dirac statistics rather than classical statistics apply, and essentially all available energy states below a particular threshold determined by the number density of carriers are filled. Accordingly, the spectrum in this case tends to flatten after a sharp rise at the band gap energy, dropping off for energies above the quasi-Fermi level [11].

Aside from the probing band-to-band transitions, PL spectroscopy can also provide information on donor/acceptor levels and exciton energies. Excitons occur when electrons and holes form a pair coupled via their coulomb attraction after an electron is excited to the valence band. The two form an essentially hydrogenic system at the energy of the bandgap less the exciton binding energy, given by the equation

$$E_{exciton} = E_g - \frac{R_x}{n^2},$$

where R_x is the Rydberg for excitons in the medium and *n* the principle quantum number [11]. Impurity scattering tend to spoil them by preventing pairing of electrons and holes, causing their presence to indicate high quality in the sample of interest [12]. Their emissions tend to be exceedingly sharp, with widths on the order of a few meV, and their presence or lack thereof offers insights into the quality of the crystals analyzed.

In addition to band-to-band and excitonic transitions, those involving donors and acceptors offer insights into the impurity content of the crystals, another measure of the quality of the samples analyzed. Donor-acceptor transitions, a dominant radiative recombination process, emit photons with energies given by

$$h\nu = E_g - E_A - E_D + \frac{q^2}{\varepsilon r},$$

where E_g, E_A, and E_D are the band gap, acceptor, and donor ionization energies, respectively. The final term accounts for the coulomb interaction between the donor and acceptor sites, ε, q, and r being the relative dielectric constant in the material, the fundamental charge, and the separation in the lattice between the donor and acceptor site involved in the transition, respectively [12]. In high quality crystals, the coulomb effect on the donor-acceptor transition leads to a discrete set of donor-acceptor peaks, with peaks corresponding to larger separations ultimately overlapping and peaks of lesser separation not falling exactly where the equation above predicts due to its neglect of higher order interactions. For the closest donor-acceptor pairs in semiconductors where the donor and acceptor energies are small (a category to which $In_xGa_{1-x}As$ belongs), the coulomb interaction can push the impurity levels out of the energy gap [12]. Other impurity transitions include conduction band-to-acceptor and donor-to-valence band (often called free-to-bound transitions) at energies given by the band gap less the energy of the acceptor or donor energy, respectively, and quantum mechanical calculations predict these transitions to occur with approximately one quarter the probably of band-to-band transitions [12].

Electrical Characterization Theory

Hall measurements allow characterization of carrier content and mobility. In Hall characterization, an electric current is driven through the sample with a magnetic field oriented perpendicular, illustrated by Figure 2 below.

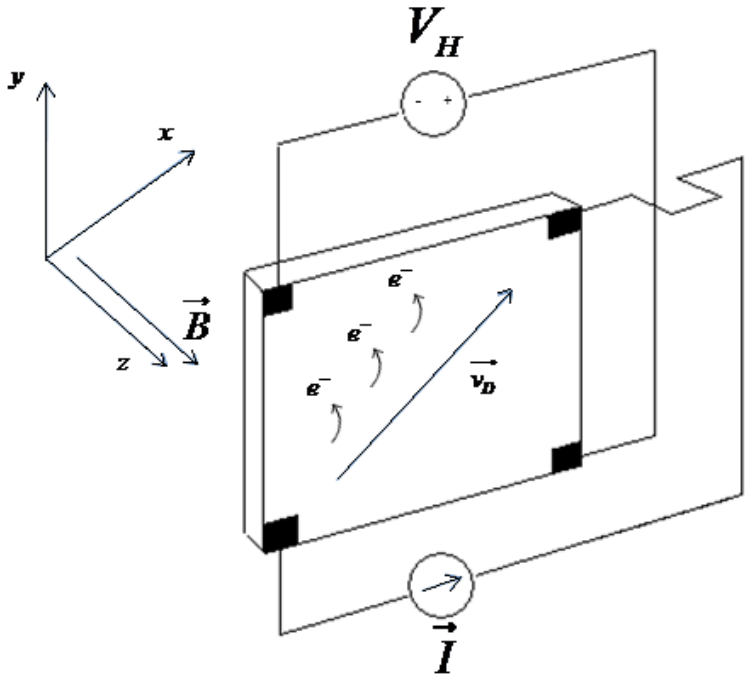

Figure 2. Schematic diagram of Hall effect measurements depicting the magnetic deflection of n-type carriers in a magnetic field.

Each charge carrier experiences the Lorentz force given by

$$\vec{F} = q\ \vec{E} + \vec{v} \times \vec{B}\ .$$

Taking the current to be in the positive $\hat{x}$ direction and the magnetic field to be in the positive $\hat{z}$ with the sample lying in the *xy*-plane, we arrive at the expression

$$E_y = v_x B_z ,$$

where E_y, referred to as the Hall field, balances the Lorentz force once the system reaches equilibrium. This equation can be rewritten

$$E_y = \frac{J_x B_x}{nq}$$

since $\vec{J} = nq\vec{v}$, and the hall coefficient is given by

$$R = \frac{1}{nq}.$$

Assuming this field to be constant, the Hall voltage is measured and given by

$$V_H = E_y \cdot y_0,$$

where y_0 is the width of the sample [13]. Armed with the Hall coefficient and conductivity, it is possible to ascertain both the carrier concentration and mobility, whereas simply measuring the conductivity, given by $\sigma = nq\mu$, only reveals their product [13]. And because the Hall coefficient depends on the sign of the charge carriers, it provides information on the relative concentrations and mobilities of the various carrier species and helps to determine whether the material is n-type or p-type, where n-type denotes a preponderance of free electrons and p-type a preponderance of holes. It is the relative concentration of donors and acceptors that determines the predominant carrier species, and as such Hall measurements can uncover the difference in donor and acceptor concentrations, assuming that at low temperatures all free carriers originate with donor impurities and all holes originate with acceptors.

Assumptions and Limitations

A variety of limiting factors affected the research. Both the optical and electrical analyses had their own set of limitations with accompanying assumptions about their effects on the data.

Some samples emitted radiation in infrared spectral bands subject to atmospheric absorption. To overcome this absorption, the path from the sample to detector was purged with high purity dry nitrogen, but in some instances (particularly for other alloys

not included in this analysis) absorption effects were still visible despite the purge. For the samples analyzed, the nitrogen purge was used for those emitting in the range of an atmospheric absorption band and it is assumed that any absorption is minor enough to maintain that data's usefulness in analysis.

In addition to atmospheric absorption's effect on the PL signal, the variation in detector response over the range of emitted wavelengths also affected the data. The InSb detector used has a detection efficiency that starts low at wavelengths around one micron and increases almost linearly to approximately 5.5 microns, at which point it drops to essentially zero. Because the PL signals have a finite bandwidth, varying on a scale perhaps only an order of magnitude narrower than the scale of the detector's variation, the detector's efficiency affects the form of the signal as it is measured and recorded. It is assumed, however, that this variation in detection efficiency is sufficient to be of little significance, particularly because the precise peak positions cannot be well defined for broad band signals.

The samples were mounted in a vacuum pumped Helitran rather than immersed in liquid helium for the PL measurements, and therefore the surface temperatures likely varied with laser power, particularly for thicker samples. In the absence of the laser beam, the sample temperature had a lower limit of approximately 10 K, leaving the extremely low temperature regime and any interesting effects therein unexamined. Compounding this limitation, the laser beam emitted light significantly above band gap energy, exciting electrons to high within the conduction band after absorption. Electrons shed this excess energy as phonons, heating the lattice. A laser emitting closer to the

samples' band gap energy, such as a 1064 *nm* Nd:YAG laser, would have resulted in less energy dissipated as heat for each electron promoted to the conduction band. It is assumed, however, that sample temperatures were relatively close to the temperatures indicated by the thermocouple on the sample mount and that the changes in temperature between measurements were accurate.

In addition to heating samples, the laser also emitted at multiple wavelengths, resulting in emission lines sometimes overlaid with the PL signal. Some of these lines were higher order harmonics from visible laser lines while others were non-lasing infrared plasma lines from the argon ion laser. In most cases these emissions were easily distinguishable from the PL signal, but in places they obscure the signal and mildly convolute analysis. These lines are labeled "laser" in the plots where they appear.

In Hall effect measurements, the sample thickness and size was the primary limiting factor. The van der Pauw method, used when samples are not square, is optimized for thin samples as close to 2-dimensional as possible. The bulk samples analyzed here, however, had significant thickness, on the order of 10% of the sample's width. It is likely that the thickness rendered the mobilities and carrier concentrations inaccurate in absolute terms. It is assumed, however, that the values given were accurate enough to give a general sense for the mobilities and carrier concentrations to the extent that they can provide insight into sample quality and doping levels, and were accurate enough that their variation with temperature illuminates the basic physics driving their variation.

II. Literature Review

Introduction

This literature review is designed to offer perspective on research involving $In_xGa_{1-x}As$ and summarizes basic understanding. Studies ranging back to the 1950's have offered insights into the earliest $In_xGa_{1-x}As$ samples grown. A variety of studies using X-ray diffraction measurements have shown that $In_xGa_{1-x}As$ obeys Vegard's law [14, 15], which states that the lattice constant of a crystalline alloy varies linearly between the lattice constants of its constituent compounds, in this case between the lattice constant of GaAs (5.65 Å) for $x = 0$ and the lattice constant of InAs (6.06 Å) for $x = 1$. Its band gap has been shown to vary between the band gaps of GaAs and InAs according to the formula $\Delta E = x \cdot \Delta E_{InAs} + (1-x)\Delta E_{GaAs} + bx\ 1-x$, where b is known as the bowing parameter and gives a quadratic correction to the interpolation between the respective band gaps of the constituent compound. Its bowing parameter has a value of 0.477 eV [16].

Crystal Growth Progress

Bulk ternary crystals similar to those studied here have been grown for several decades with varying degrees of success. Progress in the growth of $In_xGa_{1-x}As$, however, accelerated during the 1990's as a variety of techniques were attempted and improved, with particular progress coming from the Fujitsu Laboratories Ltd. [3, 5-9, 17, 18]. $In_xGa_{1-x}As$ crystals 6 mm in length with $x = 0.055 \pm 0.004$ were grown in 1990 using the liquid encapsulated Czochralski (LEC) method but suffered from a large number of

misfits and some cracks [3]. In 1995, Suzuki *et al.* reported the growth of a 13 mm $In_xGa_{1-x}As$ with $x = 0.14$ using the MCZM growth method, a significant step toward overcoming size limitations imposed by difficulties in supplying source material since the MCZM growth method allows growth of mixed crystals with fractional compositions different from the composition of the molten zone from which they are formed [9]. The group again employed the LEC method in growing bulk $In_xGa_{1-x}As$ crystals and concluded that, because of the convection virtually inevitable in melts of the size required for LEC growth and the inherent lack of uniformity that it brings, the MCZM would offer the best method for growing bulk $In_xGa_{1-x}As$ from a melt [17]. Further work by the group matured the vertical gradient freeze (VGF) technique for growing single crystals with In content varying continuously in the direction of growth to be used as seeds in the MCZM growth method once the desired In content had been reached [18], refined methods for maintaining uniform temperature along the growth interface, and yielded bulk crystals with $x \geq 0.3$ in uniform crystals 17 mm in length [7, 8] and reaching 26 mm in length for crystals of lower uniformity [6]. Others explored rotational modifications of the MCZM growth method [4, 19] and investigated the formation of polycrystalline regions due to probable supercooling in the MCZM growth method [2].

Much of the work on growth of $In_xGa_{1-x}As$ has focused on epitaxial growth and the challenges associated with growing high quality, thin layers on available substrates (usually GaAs, InAs, or InP), mentioned here briefly to provide perspective in relation to bulk growth and frame the characterization work using epitaxial $In_xGa_{1-x}As$. Liquid phase epitaxy (LPE), a melt-based growth method capable of producing layers of

exceedingly high quality, has accounted for a significant segment of this research. In 1971, T. Y. Wu and G. L. Peterson of the Stanford Electronics Laboratories applied LPE techniques to growth of electroluminescent GaAs devices to $In_xGa_{1-x}As$, studying the thermodynamics of the ternary system in the melt [15]. They determined the composition of the crystals by measuring the band gap using PL spectroscopy and successfully grew high quality epitaxial $In_xGa_{1-x}As$ layers with $x < 0.2$ on GaAs substrates and with $x > 0.7$ on InAs substrates. In a 1999 study, Soldatenov *et al.* attempted to overcome the difficulties of strain imposed by lattice-mismatching between the binary substrate and alloy and studied the growth of $In_xGa_{1-x}As$ on a porous, electrochemically etched GaAs substrate. They found that the strains in the growing layer were almost exclusively localized to within the porous substrate, which high quality growth of the epitaxial layer much like an unstrained crystal [20].

Although relatively distinct from melt-based methods, vapor phase epitaxy (VPE) is also a common technique for ternary alloy growth. In VPE, the semiconductor constituents are generally bonded to other (often organic) molecules in vapor phase. These organic compounds deposit the crystal constituents on the substrate to form the epitaxial alloy film. Vapor phase techniques offer the advantage of often yielding lower impurity concentrations relative to melt-based methods that tend to incorporate impurities from their crystal growth containers, but they generally do so at higher cost. A variety of papers study the use of a range of molecular sources for the arsenic in the alloy, primarily comparing the impurity concentrations associated the different molecular sources [21-23], and other research has examined the effects of substrate temperatures on epitaxial

crystal growth in an effort to further understand metastable alloys and their formation [24].

Optical Characterization

A great deal of the PL work on $In_xGa_{1-x}As$ has focused on epitaxial layers, particularly those lattice matched to InP with an indium mole fraction of 0.53. In their 1990 study of metalorganic vapor phase epitaxy grown $In_{.53}Ga_{.47}As$ lattice-matched to InP, Abdalla *et al.*. found an exceedingly sharp band-to-band transition with a full width at half maximum (FWHM) of 3.1 meV, demonstrating the high crystal quality attainable through vapor phase epitaxy in alloys grown without lattice mismatch [22]. Wei Gao *et al.*., in their study examining $In_xGa_{1-x}As$ lattice matched to InP and grown via liquid phase epitaxy using rare earth gettering agents, observed a similar band-to-band transition with a FWHM of 4.5 meV in samples grown from a Yb-treated melt and a FWHM of 5.5 meV with less intensity for those without the Yb-treated melt [25]. They also observed a broader, far less intense peak attributed to a band-to-acceptor transition, the increased width and appearance of impurity-related emissions demonstrating the increased difficulty associated with melt-based growth methods.

In studies examining crystal defects, Raisanen *et al.* used PL spectroscopy to examine deep states created by misfit dislocations at heterojunctions between GaAs and low indium content (x=0.08-0.1) $In_xGa_{1-x}As$, finding their emissions to be unrelated to native defects and strongly correlated to strain relaxation [26]. In a similar study involving $In_xGa_{1-x}As$ (x=0.5- 0.54) lattice matched (or nearly lattice matched) to InP, F. R. Bacher found a lattice-related defect level present through all compositions (at times

even for the lattice matched x= 0.53) with energy on the order of 0.1 eV and decreasing with rising Ga content [27]. Islam *et al.*. performed a study using micro-Raman and PL spectroscopy on MCZM grown $In_{0.3}Ga_{0.7}As$ in which crystal composition had fluctuated and caused polycrystallization throughout the crystal [2]. The mico-Raman spectroscopy compared the strength of the longitudinal and transverse optical phonons associated with both GaAs and InAs as composition varied through the sample, and the PL spectra taken at 20 μm spacing supported the micro-Raman findings in its diagnosis of polycrystlization driven by fluctuating crystal composition.

Electrical Characterization

A broad range of studies have examined $In_xGa_{1-x}As$ through Hall effect measurements. Abdalla *et al.* report a room temperature mobility of 11,200 $cm^2/(Vs)$ and a 77 K mobility of 57,000 $cm^2/(Vs)$ for $In_{0.53}Ga_{0.47}As$ lattice-matched to InP, reasonably typical mobilities for a quality $In_xGa_{1-x}As$ film with approximately equal In and Ga content [22]. Watanabe *et al.* examined the effects of annealing on epitaxial layers of $In_xGa_{1-x}As$, finding that annealing above 700 ºC reduced carrier concentration and increased mobility, most likely through the deactivation of Si donors [28]. In studies devoted to carrier lifetimes and mobilities in samples subjected to ion irradiation for fast optoelectronic applications, Mangeney *et al.* found that the mobility could undergo a reduction by a factor of 50 without increasing carrier concentrations [29], and Joulaud *et al.* were able to differentiate the defects associated with Au^+ and H^+ ions [30]. A variety of papers have reported the impact of buffer layers and growth conditions on samples' electrical properties. These papers examined the combined effects of various scattering

mechanisms on the mobility of $In_{0.53}Ga_{0.47}As$ lattice-matched to InP [31], investigated variations in mobility with InAlAs buffer presence and crystal composition and find an increase in mobility with increasing indium content and an increase in mobility with buffer layer presence [32], and compared mobilities for growth on different substrate crystal planes and temperatures [33]. Others examine the effect of gettering on mobility in melt growth methods. Gao *et al.* found a drop in carrier concentration and an increase in mobility with use of Gd as a gettering agent [25], and a study by Dhar *et al.* noted a drop in carrier concentration without a significant change in mobility using Er as a gettering agent [34]. Research by Gorelenok *et al.* confirmed reductions in impurity content with the use of rare earth gettering agents and explored implications for device applications [35]. By discerning carrier concentrations and carrier mobilities, Hall effect measurements offer significant insights into fundamental material parameters, making the technique a powerful diagnostic tool.

Summary

A considerable body of research on $In_xGa_{1-x}As$ has been built since the late 1950's. The majority of the characterization research, particularly the studies focusing on the optical and electrical properties, has applied to epitaxial layers, and within this body of work a large portion has focused on $In_{0.53}Ga_{0.47}As$ lattice-matched to InP substrates. Characterization work with bulk $In_xGa_{1-x}As$ has relied primarily on techniques such as X-ray diffraction and focused primarily on crystal composition and uniformity. Much of this research has focused on crystals of low to medium In content. It is therefore relevant

to undertake research examining the optical and electrical properties of bulk $In_xGa_{1-x}As$ of high In content.

III. Experiment

Chapter Overview

This chapter outlines the experimental methods used to characterize the $In_xGa_{1-x}As$ samples studied. It outlines the basic setups and parameters used with the aim of illuminating how the research was performed and allowing experiments to be repeated.

Experimental Procedures: Photoluminescence

Samples were mounted in a Helitran vacuum pumped to approximately 20 mili-Torr and cooled to temperatures approaching 10 K using evaporation of liquid helium. Crycon thermal grease was used to create thermal contact with and attach the samples to the Helitran. A muli-line argon ion laser with a principle wavelength of 5145 Å was used for optical excitation, and the beam was passed through an optical chopper running at approximately 170 Hz before reaching the sample. Laser power was measured between the optical chopper and the Helitran before any measurements for which laser power had changed, and after initial measurement the power was assumed to remain stable. Two calcium fluoride lenses, the first a 10 cm focal length lens to collimate the emissions and the second a 30 cm focal length lens to focus the collimated beam, collected and focused the luminescence on the entrance slit of the spectrometer, a 0.75 *m* scanning monochrometer.

For samples emitting in wavelength ranges prone to atmospheric absorption, the path from the sample to the monochrometer and the monochrometer were purged with high-purity, dry nitrogen. The monochometer collected the emitted spectra using a

Teledyne Judson Technologies J10D InSb detector. The detector was liquid nitrogen-cooled and operated with a 12 V bias. Depending on the wavelength range of the emissions, an SP35 cold filter was used to increase the signal-to-noise ratio by blocking background IR radiation outside of the 1.7 – 3.5 μm range. The detector's output was fed via a preamplifier to a Lock-In amplifier which registered signals that varied with the optical chopper's frequency. These signals were then recorded on a computer using SPEX software for analysis. Table 1 summarizes the parameters used in PL experiments, and Figure 3 presents a schematic diagram of the setup.

Sample	**N_2 Purge**	**Integration Time**	**Grating**	**Cold Filter**	**Δλ ***
InAs WT 524-10_1 x=1	off	1 s, 0.25 s**	$\lambda_{blaze} = 6\mu m$ 150 grooves/mm	off	2 *nm*
IGA 061206-6 x = .99	on	3.5 s	$\lambda_{blaze} = 2.6\mu m$ 300 grooves/mm	off	2 *nm*
IGA 052406-4_1_1 x = 0.926	on	0.25 s	$\lambda_{blaze} = 2.6\mu m$ 3 00 grooves/mm	on	2 *nm*
IGA 052406-2_2 x = 0.91	on	0.25 s	$\lambda_{blaze} = 2.6\mu m$ 3 00 grooves/mm	on	2 *nm*
IGA 052406-1_2_1 x = 0.821	on	0.1 s	$\lambda_{blaze} = 1.6\mu m$ 6 600 grooves/mm	on	2 *nm*
IGA 041506-1_2 X = 0.75	off	0.3 s	$\lambda_{blaze} = 1.6\mu m$ 6 600 grooves/mm	on	1 *nm*

* change in wavelength between intensity measurements

** 1 second integration time for power dependent measurements, 0.25 seconds for all others

Table 1. Samples studied and corresponding experimental parameters used in photoluminescence measurements

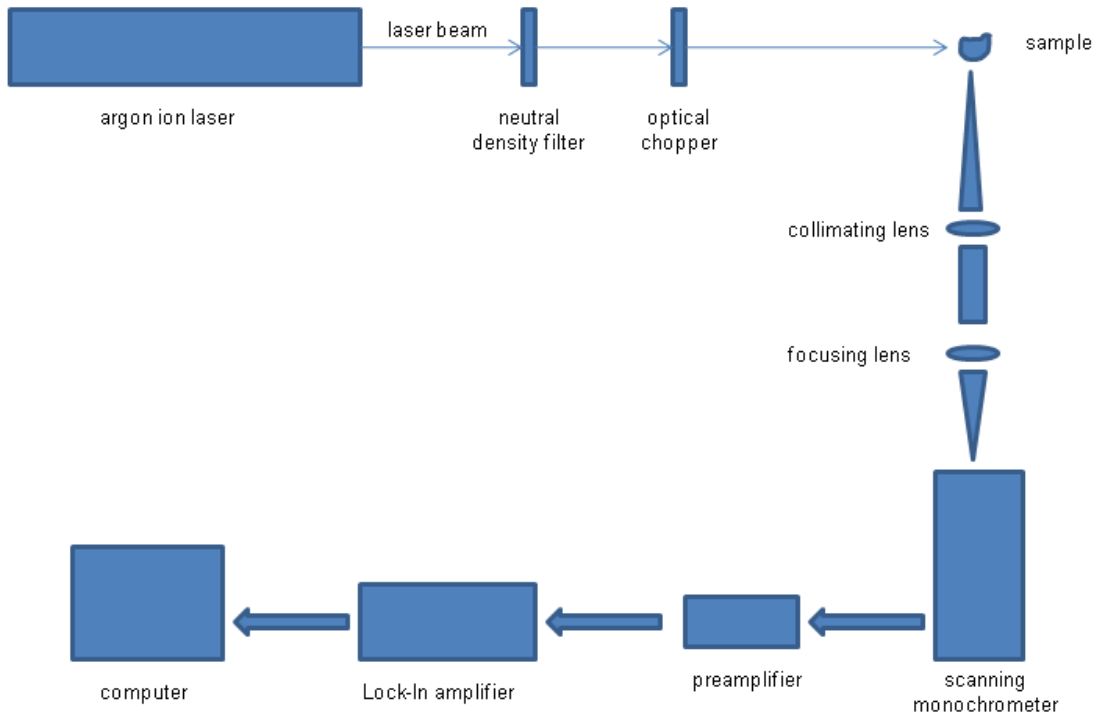

Figure 3. Photoluminescence measurement setup schematic diagram

Experimental Procedures: Hall Effect

Low temperature Hall effect measurements were performed with a Lake Shore Hall Measurement system using the van der Pauw method. Ohmic indium contacts were applied using an ultrasonic soldering iron. Samples were mounted on a helium cooled cold head inside of a vacuum chamber to prevent condensation. At the outset of measurements, a voltage vs. current test was run to ensure the ohmicity of the contacts. Following the voltage vs. current measurement, Hall effect measurements were performed using a 5 kG magnetic field over temperatures ranging from 10 or 15 K (depending on the sample) to 300 K. Temperatures were incremented by 5 K for

measurements from 10 to 50 K, 10 K for measurements from 50 to 120 K, and 20 K for measurements from 120 to 300 K.

IV. Results and Analysis

Overview

Photoluminescence and Hall effect measurements revealed broad, band-edge luminescence, moderate n-type doping, and mobility values commensurate with those of similar samples, offering insights into the quality of the crystals grown. The results of the PL and Hall measurements are compared and corroborated, with Hall measurements, in particular, serving as a tool to interpret PL spectra.

Several band-edge transitions appeared in the PL spectra, and all displayed the broadening associated with samples of moderate to high impurity content. The band-to-band peaks generally followed the predicted band gap as crystal composition varied, shown in Figure 4 below. Because the temperature on the surface of the sample is not known and because of the propensity for impurity concentrations to affect the position of the band-to-band peak through band tailing or band filling, the information plotted here does not allow precise determination of crystal composition but shows at least that the sample compositions were strongly correlated to the compositions reported by the crystal grower.

In addition to band-to-band transitions, shallow and deep donor-acceptor pair transitions were also observed. These transitions were not visible in all of the samples studied, and several samples distinguishably exhibited only band-to-band transitions, but behaviors of these emissions were relatively consistent from sample to sample when they were present. The samples $In_{0.75}Ga_{0.25}As$, $In_{0.82}Ga_{0.18}As$, and $In_{0.93}Ga_{0.07}As$ in particular

showed especially similar behavior in their power dependent and temperature dependent PL spectra.

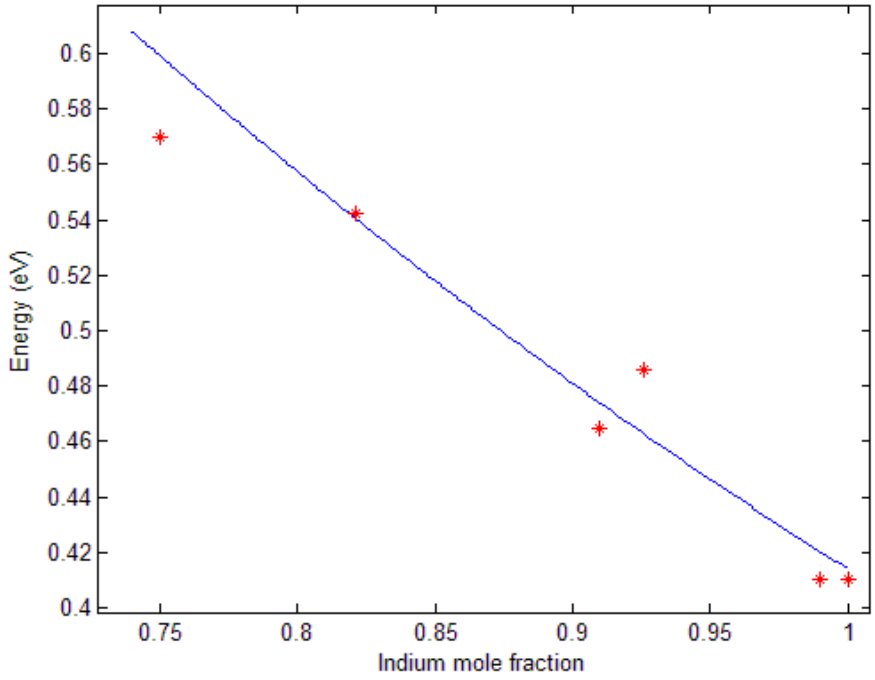

Figure 4. Low temperature (10-12 K) band-to-band emission peak energies plotted along with the predicted 12 K band gap in $In_xGa_{1-x}As$ alloys for indium mole fractions varying from 0.75 to 1

Hall effect measurements revealed moderate n-type doping, with all samples having low temperature carrier concentrations on the order of 10^{16} cm^{-3}. Carrier mobility values were found to be on the order of 10^4 $cm^2/(V \cdot s)$, within the range expected for $In_xGa_{1-x}As$ of the indium content present in this study. Table 2 summarizes the findings of the Hall effect measurements.

Sample $In_xGa_{1-x}As$	Carrier Concentration (cm^{-3})	Mobility 15 K $cm^2/(V\cdot s)$	Mobility 80 K $cm^2/(V\cdot s)$	Mobility 300 K $cm^2/(V\cdot s)$
IGA 041506-1_2 x = 0.75	1.5×10^{16} (10 K)	1.3×10^4	$1.5\cdot\times10^4$	4.8×10^3
IGA 052406-1_2_1 x = 0.82	$2.8\cdot10^{16}$ (15 K)	1.5×10^4	1.6×10^4	1.1×10^4
IGA 052406-2_2 x = 0.91	$3.7\cdot10^{16}$ (10 K)	1.6×10^4	1.8×10^4	1.2×10^4
IGA 052406-4_1_1 x = 0.93	$4.1\cdot10^{16}$ (10 K)	1.4×10^4	1.6×10^4	1.1×10^4
IGA 061206-6_2 x = .99	$9.6\cdot10^{16}$ (10 K)	1.8×10^4	2.1×10^4	1.4×10^4
InAs WT 524-10_1 x = 1	$2.1\cdot10^{16}$ (15 K)	3.5×10^4	4.7×10^4	3.3×10^4

Table 2. Low temperature (10-15 K) carrier concentrations and Hall mobilities at varied temperatures for each of the samples studied.

As expected given the greater carrier mobility of InAs than GaAs, mobility increased with increasing indium content. Mobilities in all samples increased from their low temperature values but began to drop above approximately 100 K, as suggested by the chart above in which the 80 K mobility is the highest presented for each sample. (Mobilities at 80 K were reported to facilitate comparison with results of other studies since mobility values are often reported at liquid nitrogen temperature.) The sharp jump in mobility from $In_{0.99}Ga_{0.01}As$ to InAs relative to the incremental increases in mobility between the other samples illustrates the effect of alloying. Alloying tends to reduce the mobility through both the alloy scattering inherent in any mixed crystal and through the drop in crystal quality associated with the more challenging growth process.

Results for $In_{0.75}Ga_{0.25}As$ (IGA 041506-1_2)

Hall effect measurements for $In_{0.75}Ga_{0.25}As$ showed moderate n-type doping, with a low temperature carrier concentration of 1.5×10^{16} cm^{-3}. Hall mobility (shown below in

Figure 5) was driven by ionized impurity (or space charge) scattering at low temperature with optical phonon scattering becoming dominant as temperature rose. Alloy disorder scattering, caused by the non-periodicity inherent to the potential experienced by a carrier in a mixed composition lattice, also affects mobility. Its behavior and that of ionized impurity scattering both have the same temperature dependence however, making it impossible to separate the behavior of these two mechanisms [23].

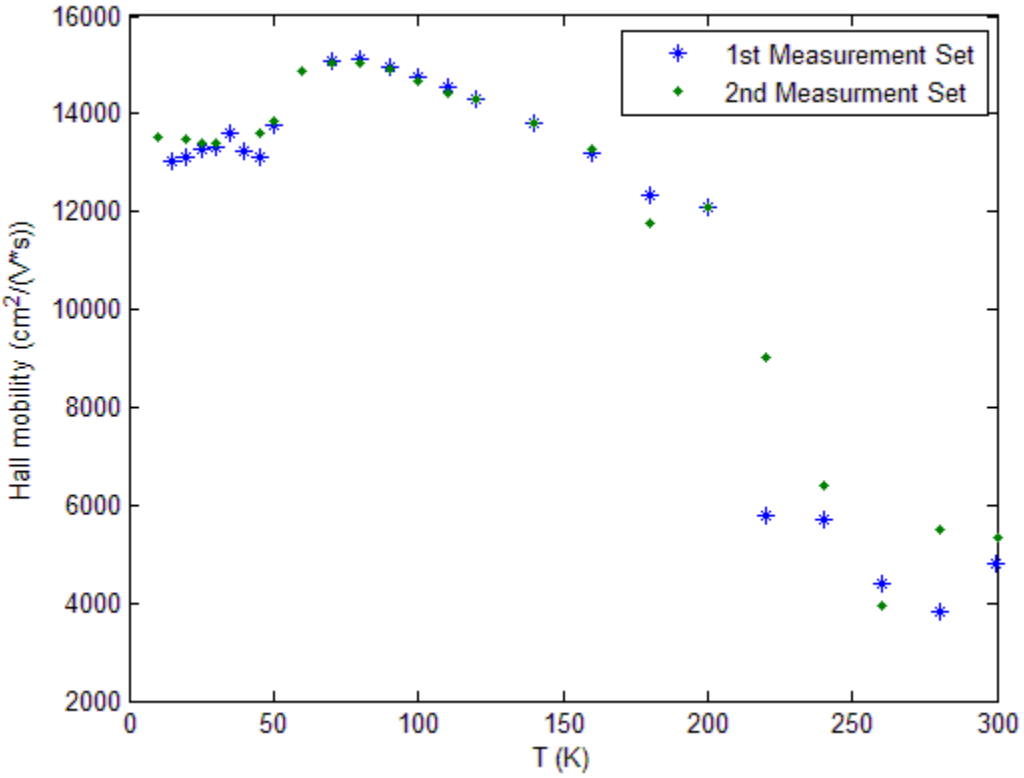

Figure 5. Temperature dependent Hall mobility of $In_{0.75}Ga_{0.25}As$

Because of the fluctuations apparent in the mobility data presented above, a second measurement was performed under identical conditions to eliminate some of the uncertainty in the behavior. In both measurement sets, outliers occurred in which both

the mobility and carrier concentration at a particular temperature were nearly an order of magnitude or more different from the values at neighboring temperatures. With reasonable certainty that such measurements were not due to any interesting physics, these data points were removed.

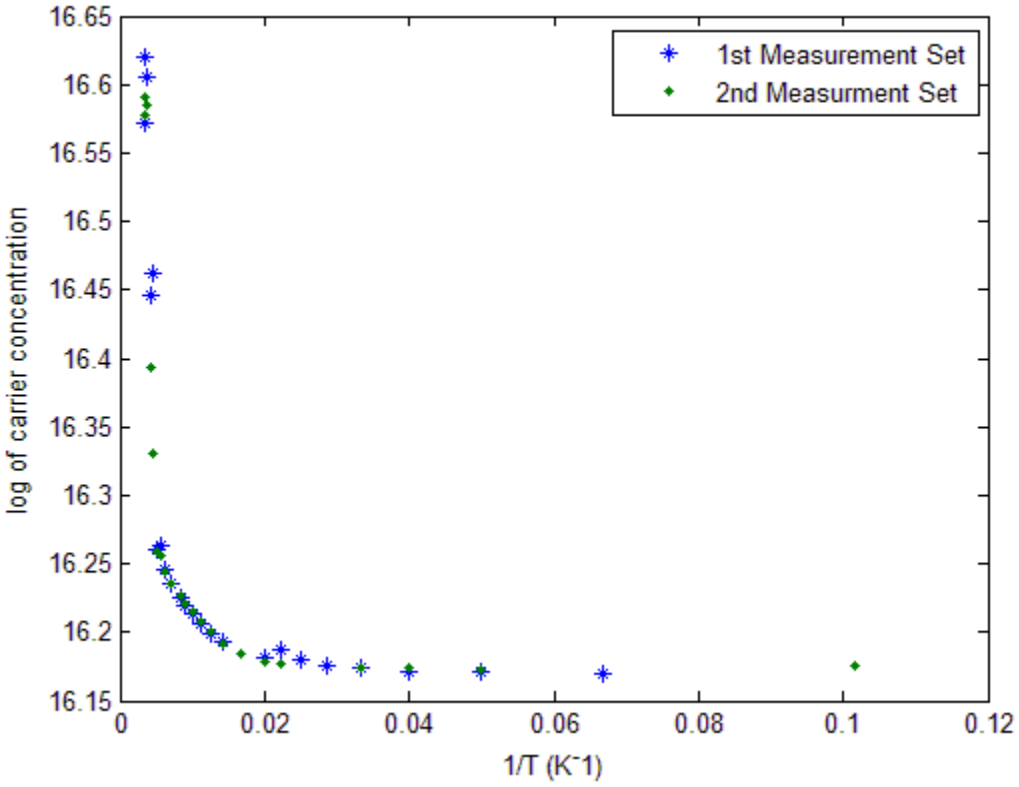

Figure 6. Log of carrier concentration vs. inverse temperature for $In_{0.75}Ga_{0.25}As$

Temperature dependent carrier concentrations, shown above in Figure 6, suggest two origins for carriers. At low temperatures, degenerate carriers from shallow donors populated the conduction band, and above approximately 50 K carriers from deep donor levels became appreciable in the conduction band. The increase in carrier concentration, which occurred between approximately 50 and 100 K in all samples studied, bore strong resemblance to an onset of intrinsic carriers excited from the valence band. The intrinsic

carrier concentration, however, was calculated to be only 1.2×10^{11} cm^{-3} at 200 K and 7.1×10^{13} cm^{-3} at 300 K, far too low to account for the increase observed. Additionally, the slope of the natural log of carrier concentration versus inverse temperature should provide a good estimate of the band gap when intrinsic carriers are appreciable. The slope here, however, underestimates the band gap by an order of magnitude, another indication that these carriers arose from a deep donor level.

Pl data is displayed in Figure 7 and Figure 8 on the following pages with additional data shown in Appendix I. Figure 7 shows laser excitation power dependent PL spectra taken at 13 K with laser power varying from 100 to 600 mW, and Figure 8 shows temperature dependent PL spectra taken with a laser excitation power of 200 mW. These figures show three distinct peaks at 0.570, 0.551, and 0.533 eV in 13 K spectra with 100 mW and 200 mW laser excitation. Based on the behavior of these peaks, the 0.570 eV peak has been classified as a band-to-band (B-B) transition, the 0.551 eV peak a shallow donor-acceptor pair (D_1-A) transition, and the 0.533 eV peak a deep donor-acceptor pair (D_2-A) transition. The behavior of these peaks shows strong similarities to the PL peaks of $In_{0.93}Ga_{0.07}As$ (IGA 052406-4_1_1) and $In_{0.82}Ga_{0.18}As$ (IGA 052406-1_2_1), which are discussed in subsequent sections.

The highest energy PL peak at 0.570 eV showed strong stability with increasing temperature and grew significantly as excitation power was increased. In power dependent spectra, this 0.570 eV peak started out as an unresolved shoulder on the shallow donor-acceptor pair transition under 100 mW excitation and became stronger

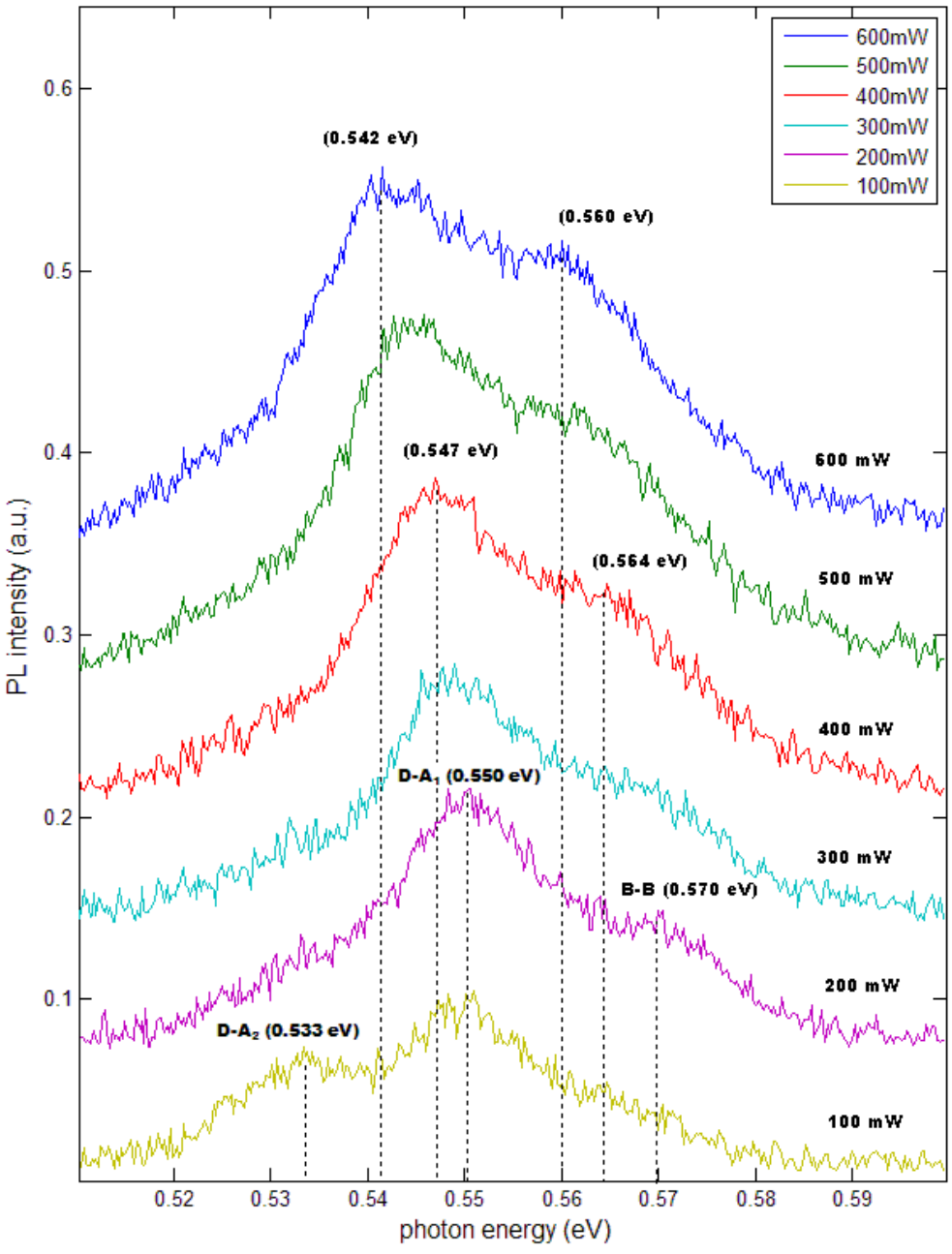

Figure 7. Laser excitation power dependent photoluminescence spectra of $In_{0.75}Ga_{0.25}As$ at 13 K

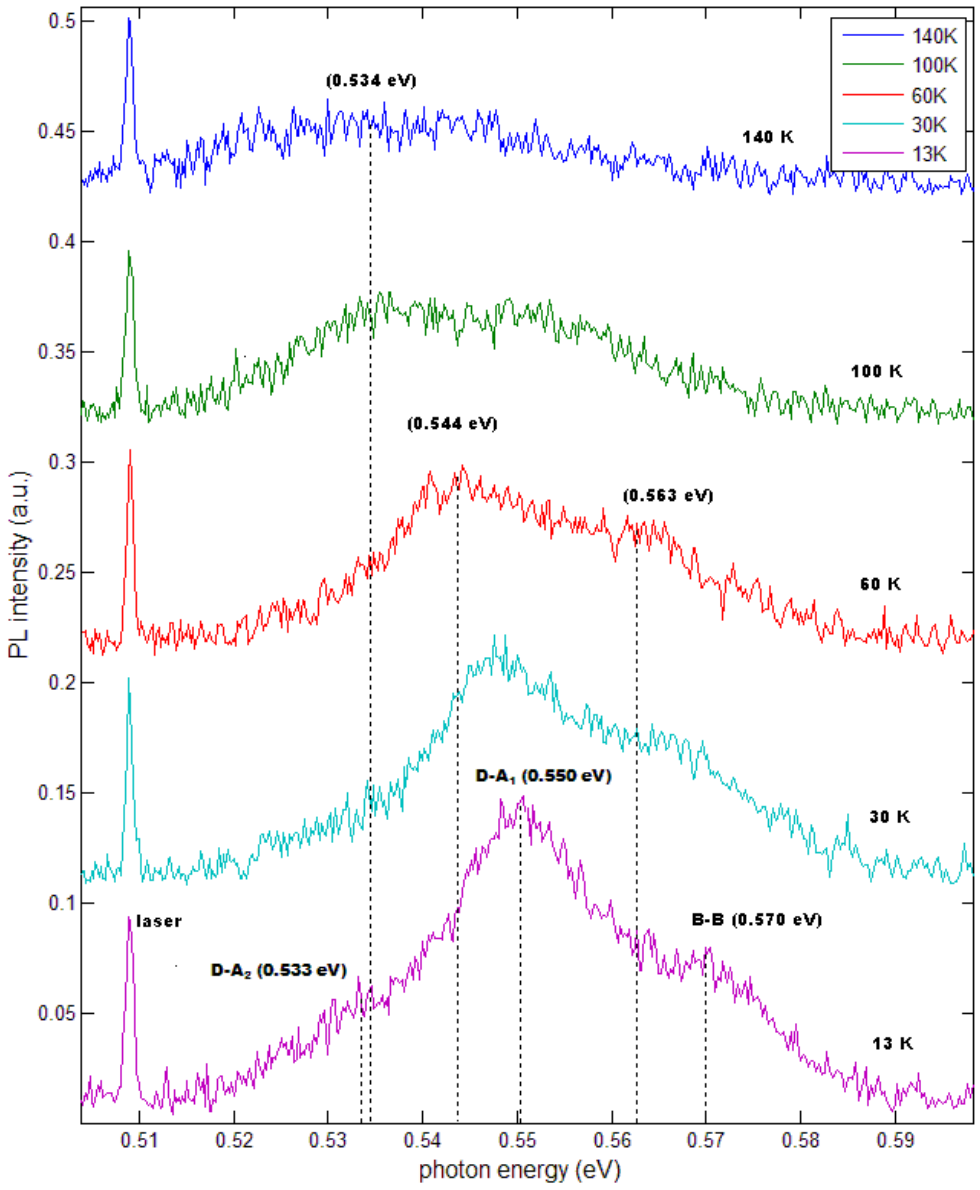

Figure 8. Temperature dependent photoluminescence spectra of $In_{0.75}Ga_{0.25}As$ with 200 mW excitation power

relative to the D_1-A transition until 300 mW. Above 300 mW, both peaks grew in tandem and shifted toward slightly lower energy, most likely because of a decrease in the band gap due to surface heating.

The second peak at 0.551 eV, the shallow donor-acceptor pair transition, showed good thermal stability with increasing laser excitation power and temperature. Only at approximately 100 K did the B-B transition match the D_1-A intensity, and at 140 K the D_1-A peak and the band-to-band peak were indistinguishable. The D_1-A position in the spectrum at 13 K under 200 mW laser excitation indicates donor and acceptor ionization energies adding up to19 meV, a value within the realm of possibility for a narrow band gap material such as the present sample. This D_1-A peak persisted with increased temperature to a far greater extent than the D_1-A transitions observed in the other samples exhibiting otherwise similar behavior. This sample had the lowest carrier concentration (1.5×10^{16} cm^{-3} at 10 K versus 2.8×10^{16} cm^{-3} for $In_{0.82}Ga_{0.18}As$ at 15 K and 4.1×10^{16} cm^{-3} for $In_{0.93}Ga_{0.07}As$) of those considered, and this low carrier concentration may have occurred as much because of compensation from an increased acceptor content as from a decreased donor concentration. With an increased acceptor concentration, the lower carrier concentration need not reflect a decreased donor content but instead could point toward a greater prevalence of donor-acceptor pairs. An increased prevalence of donors could then explain the greater thermal stability of this D_1-A peak.

The lowest energy peak, observed at 0.533 eV, is classified as a deep donor-acceptor transition. This D_2-A peak displayed ambiguity in its behavior as laser power increased, not clearly shifting to higher energy as donor-acceptor transitions are apt to do,

but some of this difficulty arises because this transition was a shoulder peak not clearly resolvable from the D_1-A transition. At 0.533 eV, this D_2-A peak was 17 meV below the D_1-A peak. Assuming this D_2-A transition involves the same acceptor type as the D_1-A transition, the deep donor ionization energy must be 17 meV plus the shallow donor ionization energy, a large value for donors in a narrow band gap semiconductor. In the family of samples displaying behavior most similar to that of this sample, the separation between the D_1-A transition energy and the D_2-A energy was always similar to the separation displayed here. And for all of these samples, Hall effect measurements suggested the presence of a deep donor level as previously discussed. It is because of these Hall measurements that this peak has been classified deep donor-acceptor transition.

Position dependent PL spectra, displayed below in Figure 9, showed moderate sample non-uniformity with a 5 meV maximum variation in peak position. This variation in peak position suggests a 0.4-percent compositional variation across the crystal of based on the relationship between expected band gap and sample composition.

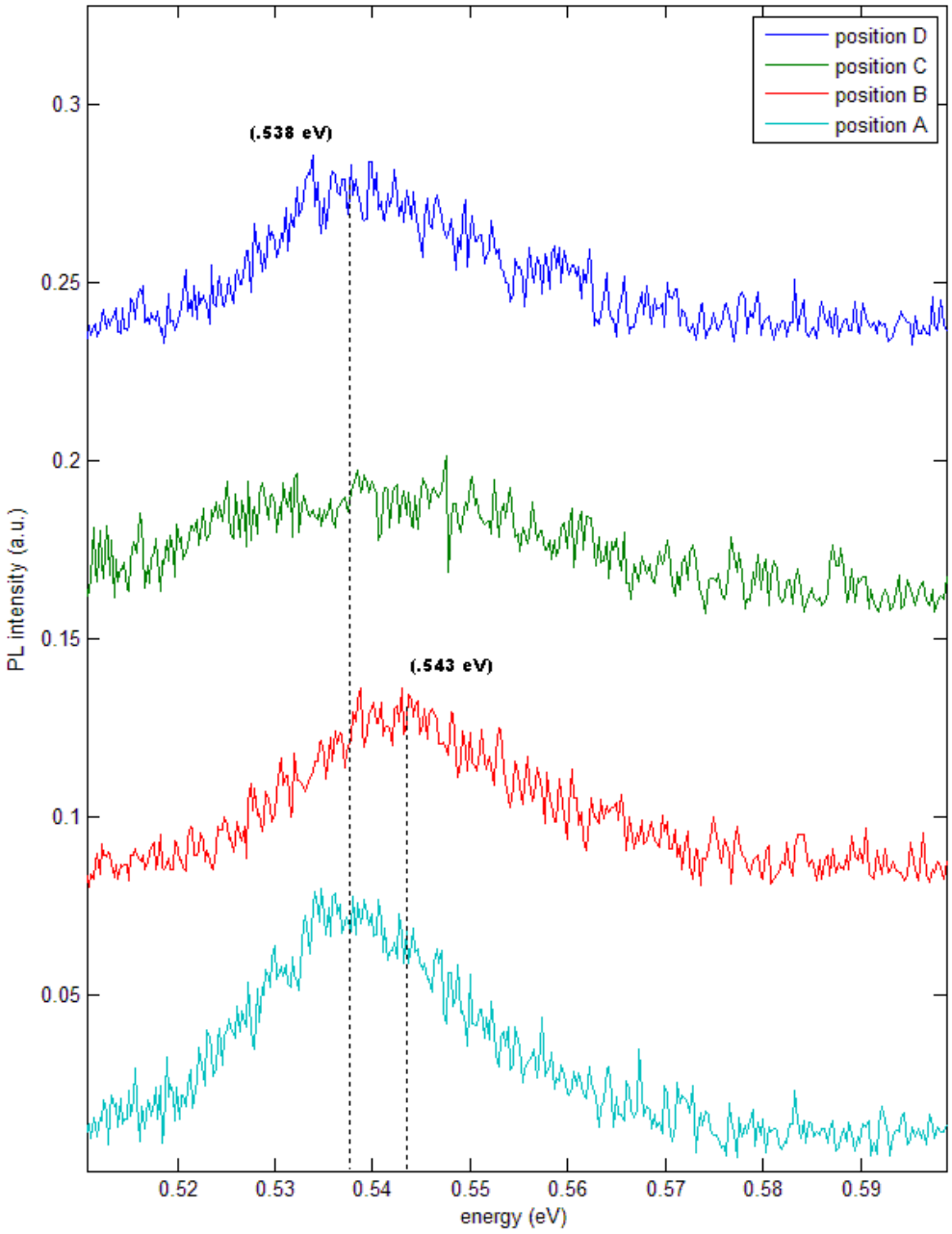

Figure 9. Position dependent measurements for $In_{0.75}Ga_{0.025}As$ at 13 K with 200 mW excitation power

Results for $In_{0.82}Ga_{0.18}As$ (IGA 052406-1_2_1)

Hall effect measurements for $In_{0.82}Ga_{0.18}As$ showed moderate n-type doping with a 15 K carrier concentration of 2.8×10^{16} cm^{-3}. Hall mobility was dominated at low temperature by ionized impurity scattering and at high temperature by optical phonon scattering, typical for the samples examined in this study. The Hall effect data for this sample (depicted in Figure 10 and Figure 11) showed fewer anomalous values than data for other samples, with the exception of the fluctuation in low temperature mobility values and the slight drop in carrier concentration at 35 K (or 0.0286 K^{-1} on the inverse temperature plot). Similar to $In_{0.75}Ga_{0.25}As$, the carrier concentration remained relatively constant until approximately 50 K at which point thermally promoted carriers from deep donor levels began to make an appreciable contribution to the total concentration.

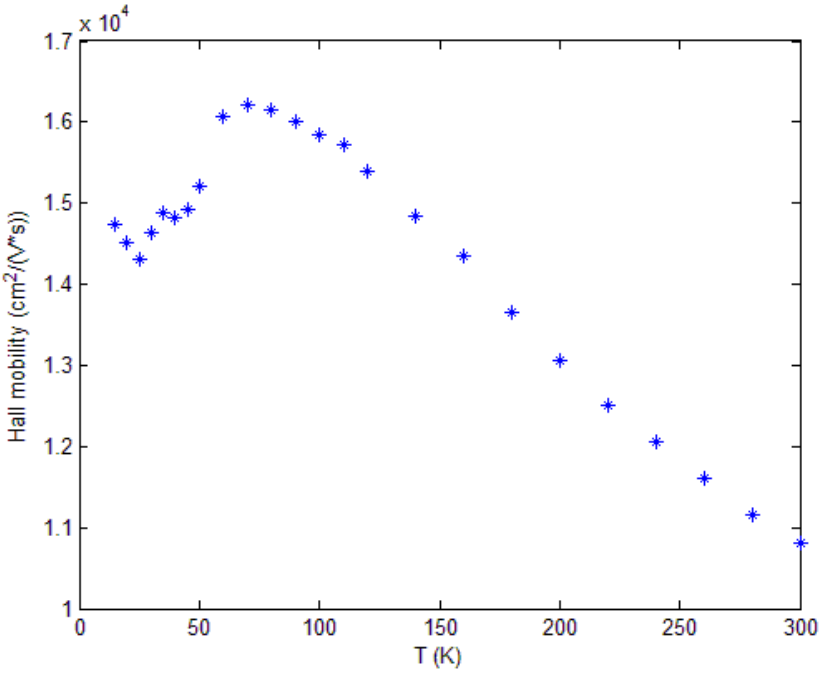

Figure 10. Temperature dependent Hall mobility of $In_{0.82}Ga_{0.18}As$

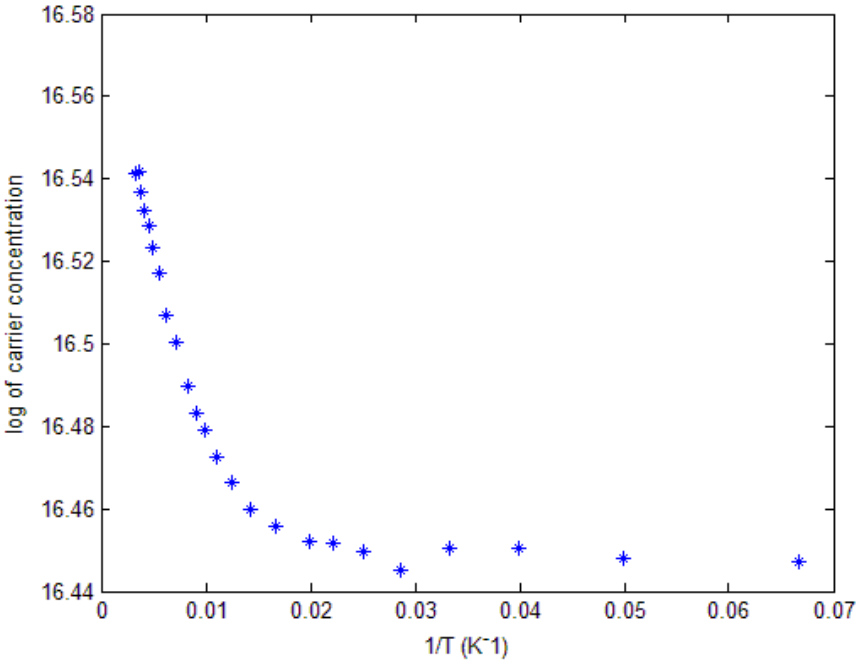

Figure 11. Log of carrier concentration versus inverse temperature for $In_{0.82}Ga_{0.18}As$

PL spectra for $In_{0.82}Ga_{0.18}As$ are displayed in Figure 12, Figure 13, and Figure 14 with additional data shown Appendix II as well. Figure 12 shows laser excitation power dependent PL spectra taken at 12 K, and Figure 13 and Figure 14 show temperature dependent PL spectra under 400 mW laser excitation power for temperatures ranging from 12 to 50 K and 50 to 130 K respectively. These spectra displayed two distinct peaks and a low energy tail, and the peak positions varied by approximately 3 meV between the temperature dependent set and the power dependent set, likely due to measurement sets on subsequent days being taken at slightly different sample positions. Peak positions are reported from temperature dependent measurement set unless otherwise specified. The highest energy peak, arising from a band-to-band transition, occurred at 0.540 eV at 12 K under 400 mW laser excitation power, shown in Figure 13.

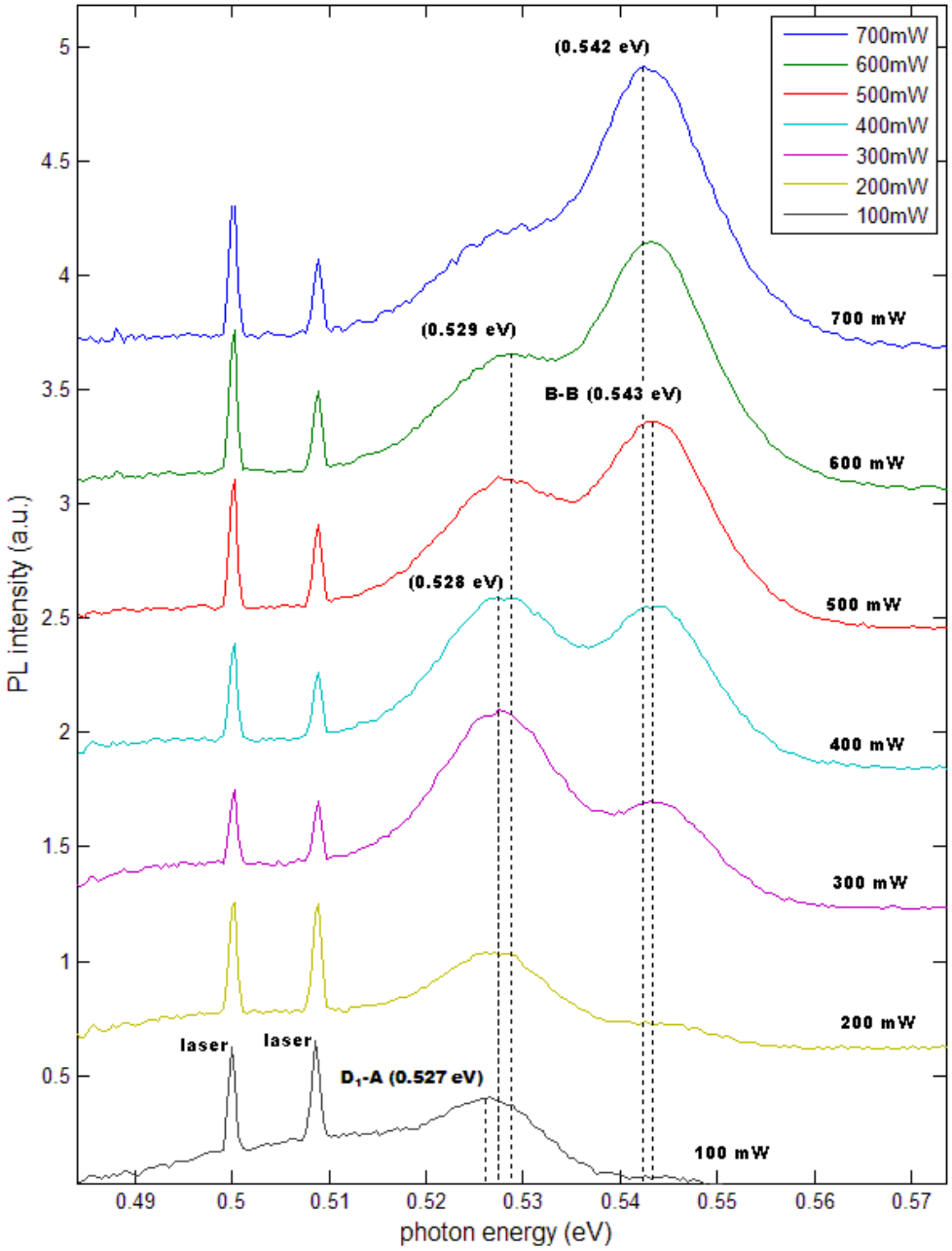

Figure 12. Laser excitation power dependent photoluminescence spectra for $In_{0.82}Ga_{0.18}As$ at 12 K

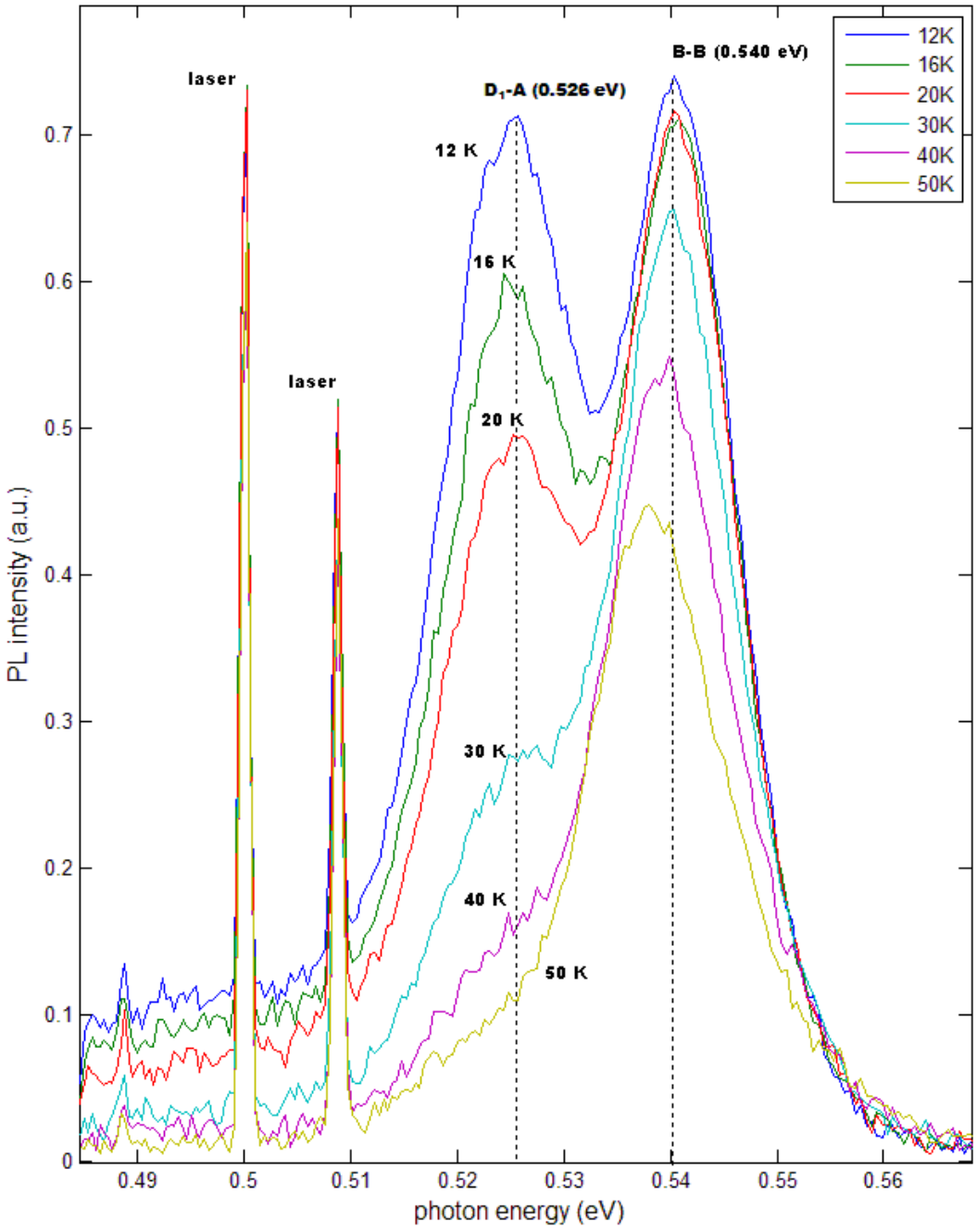

Figure 13. Temperature dependent photoluminescence spectra of $In_{0.82}Ga_{0.18}As$ with 400 mW excitation power

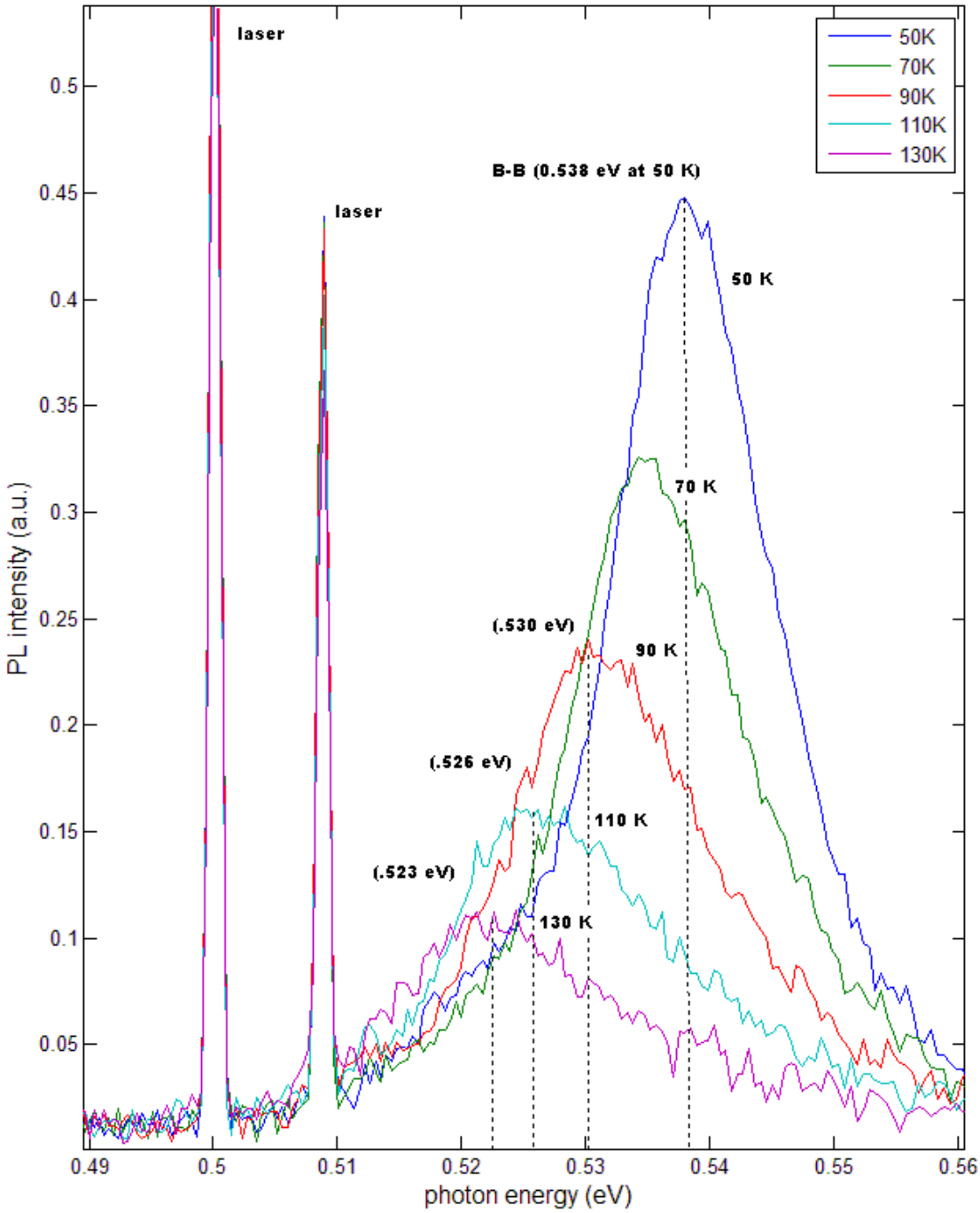

Figure 14. Temperature dependent photoluminescence spectra of $In_{0.82}Ga_{0.18}As$ with 400 mW excitation power

In power dependent measurements, this B-B transition grew significantly with increasing laser power, starting out nearly nonexistent at 100 mW and reaching approximately twice the height of the second peak (located at 0.527 eV in power dependent measurements) by 700 mW. The B-B peak underwent virtually no change in position as laser power rose, indicating good thermal contact with the Helitran and good heat conduction through the sample.

The second peak, located at 0.526 eV as shown in Figure 13, displayed common characteristics of donor-acceptor transitions, namely that it appeared to move toward higher energy with increasing laser excitation power and had low thermal stability, dropping out almost entirely by 40 K. Like other samples studied with similar behavior, specifically $In_{0.75}Ga_{0.25}As$ and $In_{0.93}Ga_{0.07}As$, this transition has been classified a shallow donor-acceptor pair transition. The sum of the acceptor and shallow donor ionization energies were therefore 14 meV. The low energy tail visible in the spectra shown in Figure 12 and Figure 13 likely originated with a deep donor-acceptor pair transition. It is classified as such due to its broad width, temperature instability, and behavior analogous to the broad low-energy peaks seen in $In_{0.75}Ga_{0.25}As$ and $In_{0.93}Ga_{0.07}As$.

Position dependent PL spectra for $In_{0.82}Ga_{0.18}As$ (presented in Appendix II) indicate varied sample composition. The band-to-band peak changed position by approximately 11 meV across the range of spectra, indicating a 0.8-percent variation in sample composition based on the relationship between sample composition and expected band gap.

Results for $In_{0.91}Ga_{0.09}As$ (IGA 052406-2_2)

Hall effect measurements for $In_{0.91}Ga_{0.09}As$ showed moderate n-type doping, with a low temperature carrier concentration of 3.7×10^{16} cm^{-3} and reasonable mobility in relation to the other samples studied. The Hall mobility, shown in Figure 15, followed the general pattern seen in other samples, rising from its low temperature values dominated by impurity scattering before being significantly affected by phonon scattering above 100 K. Carrier concentrations, displayed in Figure 16, fluctuated troublingly around 50 K but displayed the same general trend seen in other samples, beginning to rise sharply between 50 and 100 K as deep donor carriers become appreciable.

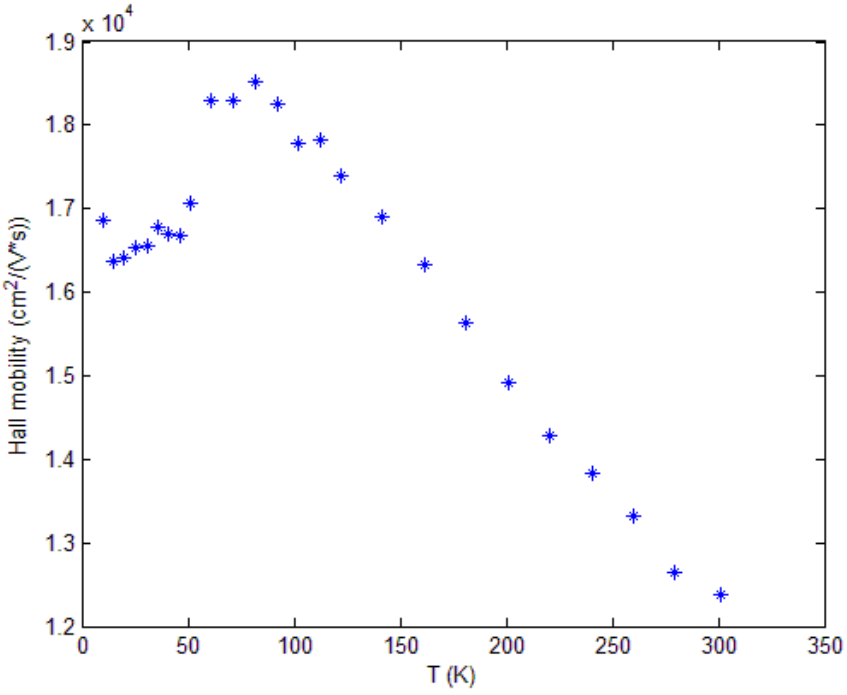

Figure 15. Temperature dependent Hall mobility of $In_{0.91}Ga_{0.09}As$

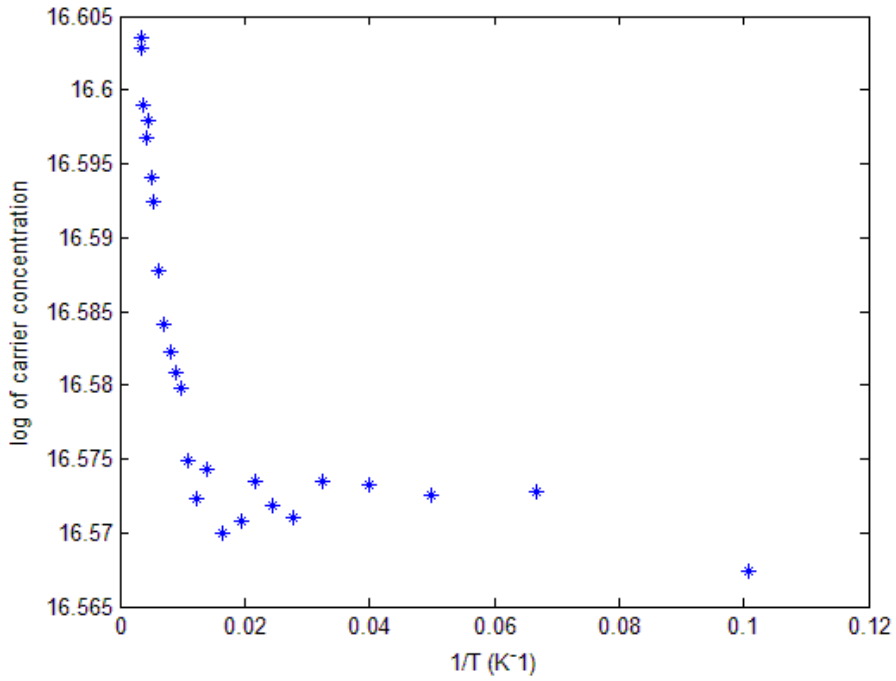

Figure 16. Log of carrier concentration vs. inverse temperature for $In_{0.91}Ga_{0.09}As$

PL spectra from $In_{0.91}Ga_{0.09}As$ (shown in Figure 17,

Figure 18, and Appendix III) present a simpler picture than those from the samples previously discussed. A single peak, likely a band-to-band transition, appeared at approximately 0.468 eV at 10 K under 200 mW excitation power, as shown in the power dependent spectra displayed Figure 17. It was marred by an atmospheric absorption line at 0.464 eV, making a meaningful determination of the peak position challenging. Despite the use of a dry nitrogen purged beamline, this drop in PL intensity is classified as an atmospheric absorption (rather than as a separation between distinct emission peaks) due to its nearly constant position, the known presence of an absorption line at the wavelengths in question, and the improbability of observing a pair of PL peaks

in which the lower energy grows with increasing laser excitation power and temperature. At higher temperatures, perhaps only

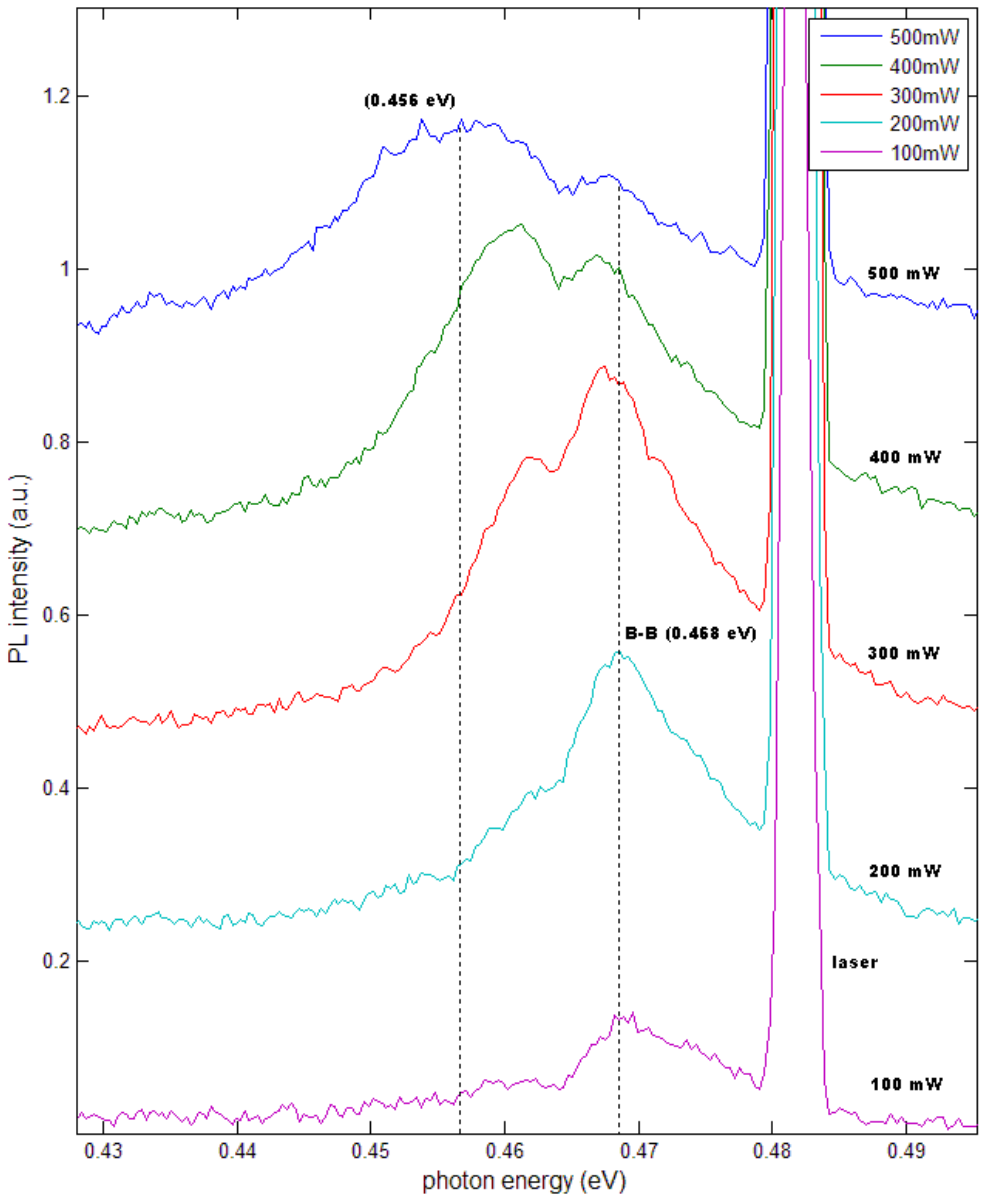

Figure 17. Laser excitation power dependent photoluminescence spectra from $In_{0.91}Ga_{0.09}As$ at 10 K

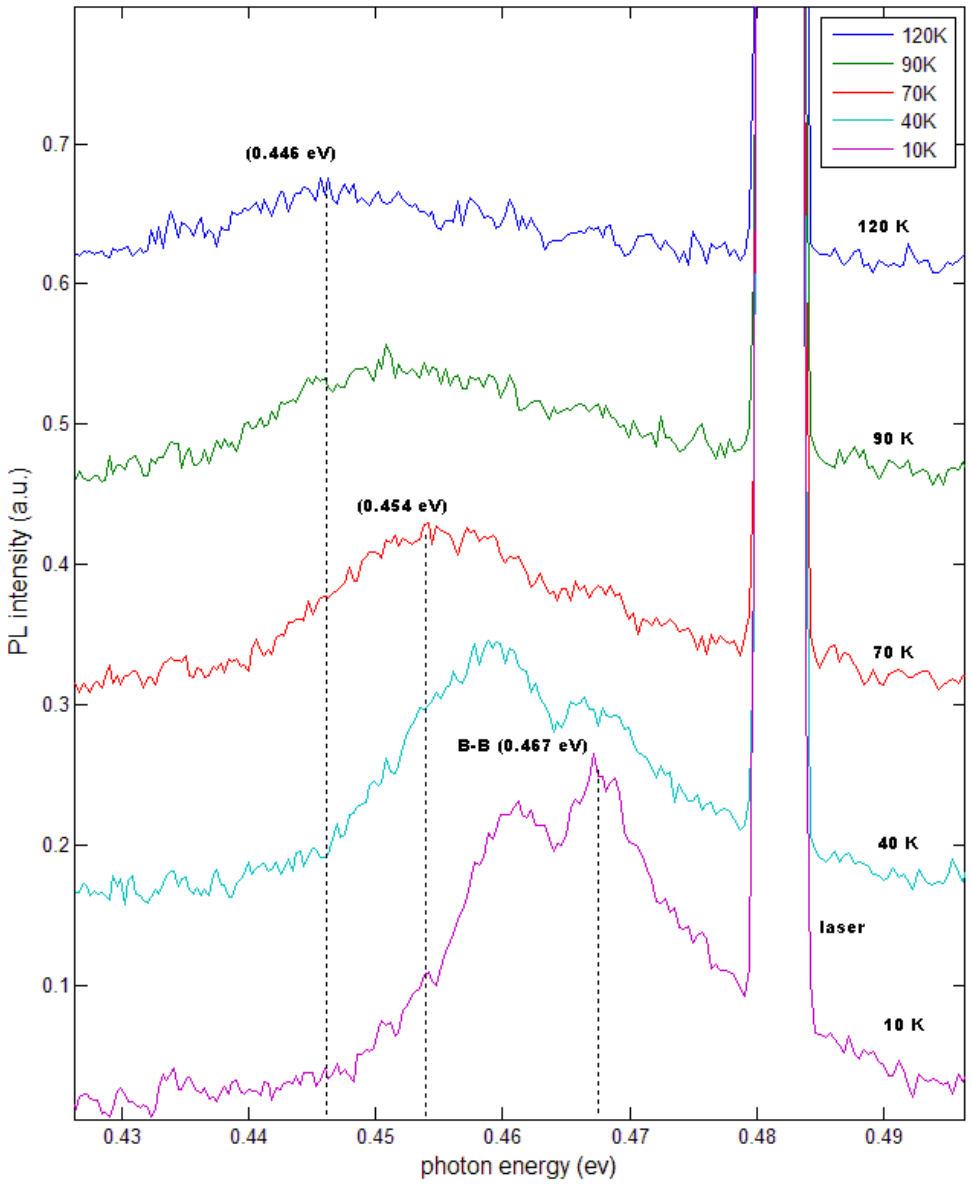

Figure 18. Temperature dependent photoluminescence spectra of $In_{0.91}Ga_{0.09}As$ with 350 mW excitation power

because the nitrogen purge had been running longer and displaced a greater fraction of the water and CO_2 in the beam line and spectrometer, the absorption was less prominent.

Power dependent measurements, displayed in Figure 17 and taken at 10 K, showed the peak position shift by approximately 15 meV from the 100 mW to the 500 mW spectra, indicating significant surface heating due to the laser excitation. Temperature dependent measurements, displayed in Figure 18 and taken under 350 mW laser excitation power, showed the band gap decreasing with rising temperature as expected. Indicative of the relationship between laser power and surface heating, the spectrum taken at 10 K under 500 mW laser excitation in the power dependent measurement set (displayed in Figure 17) showed strong resemblance to the spectrum taken at 40 K under 350 mW laser excitation in the temperature dependent measurement set (displayed in Figure 18).

Position dependent PL measurements (displayed in Appendix III) suggest that the sample is of uniform composition. Although the intensity varies across the spectra, the peak positions did not shift significantly.

Results for $In_{0.93}Ga_{0.07}As$ (IGA 052406-4_1_1)

Hall effect measurements revealed mobilities and carrier concentrations for $In_{0.93}Ga_{0.07}As$ that mirrored the behavior of the other samples studied, as shown in Figure 19 and Figure 20. Like the others examined, $In_{0.93}Ga_{0.07}As$ displayed increasing mobility

with increasing temperature until approximately 100 K at which point phonon scattering took effect as the primary mechanism limiting mobility. Similar to other samples studied (although more pronounced in this case), the mobility underwent a sharp jump between 55 and 60 K. This jump generally occurred at the point in the data sets corresponding to the changed from 5 to 10 K spacing between measurements. This sharp rise may therefore reflect a measurement anomaly rather than the physics driving the sample's behavior. This sample displayed the second highest carrier concentration among the samples studied (4.1×10^{16} cm^{-3}) and the second lowest mobility (1.4×10^{4} $cm^2/V\cdot s$) at low temperature, likely a result of the increased ionized impurity scattering associated with elevated impurity concentration.

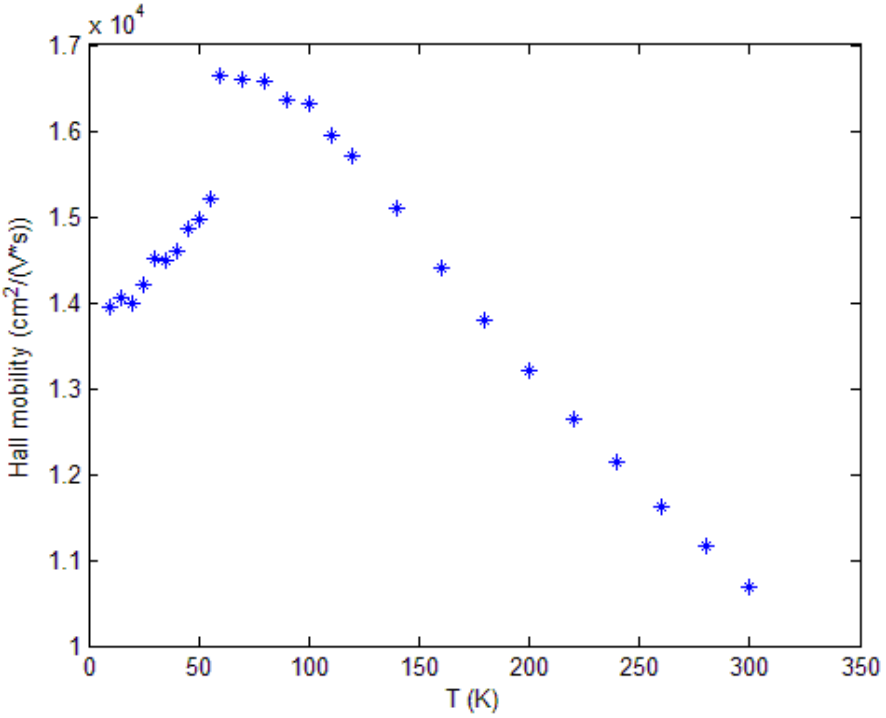

Figure 19. Temperature dependent Hall mobility of $In_{0.93}Ga_{0.07}As$

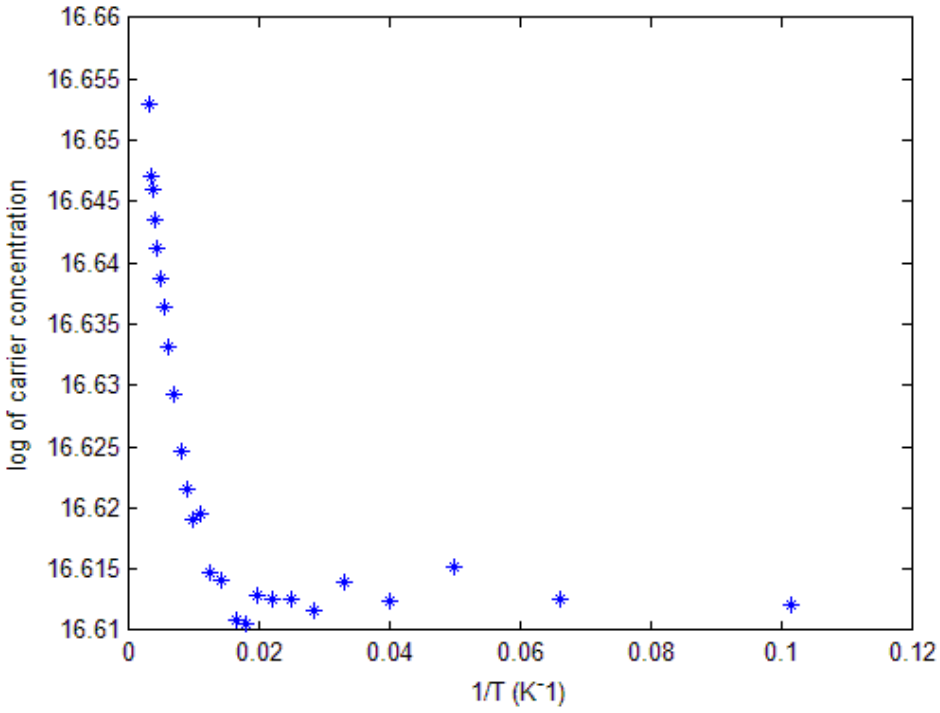

Figure 20. Log of carrier concentration vs. inverse temperature for $In_{0.93}Ga_{0.07}As$

The carrier concentration shown in Figure 20 displayed troubling fluctuations between approximately 10 and 70 K, casting doubt on the precision of the measurements. The general behavior, however, followed that of the other measurement sets with relatively flat impurity related carrier concentrations until approximately 50 K at which point carriers from deep donors became appreciable.

PL spectra for $In_{0.93}Ga_{0.07}As$ (shown in Figure 21, Figure 22, and Appendix IV) displayed three peaks with similar behavior to the PL spectra of $In_{0.75}Ga_{0.25}As$ and $In_{0.82}Ga_{0.18}As$. Figure 21 displays laser power dependent spectra at 11 K with laser power ranging from 25 to 200 mW, and Figure 22 displays temperature dependent PL spectra under 100 mW laser excitation power for temperatures ranging from 11 to 140 K.

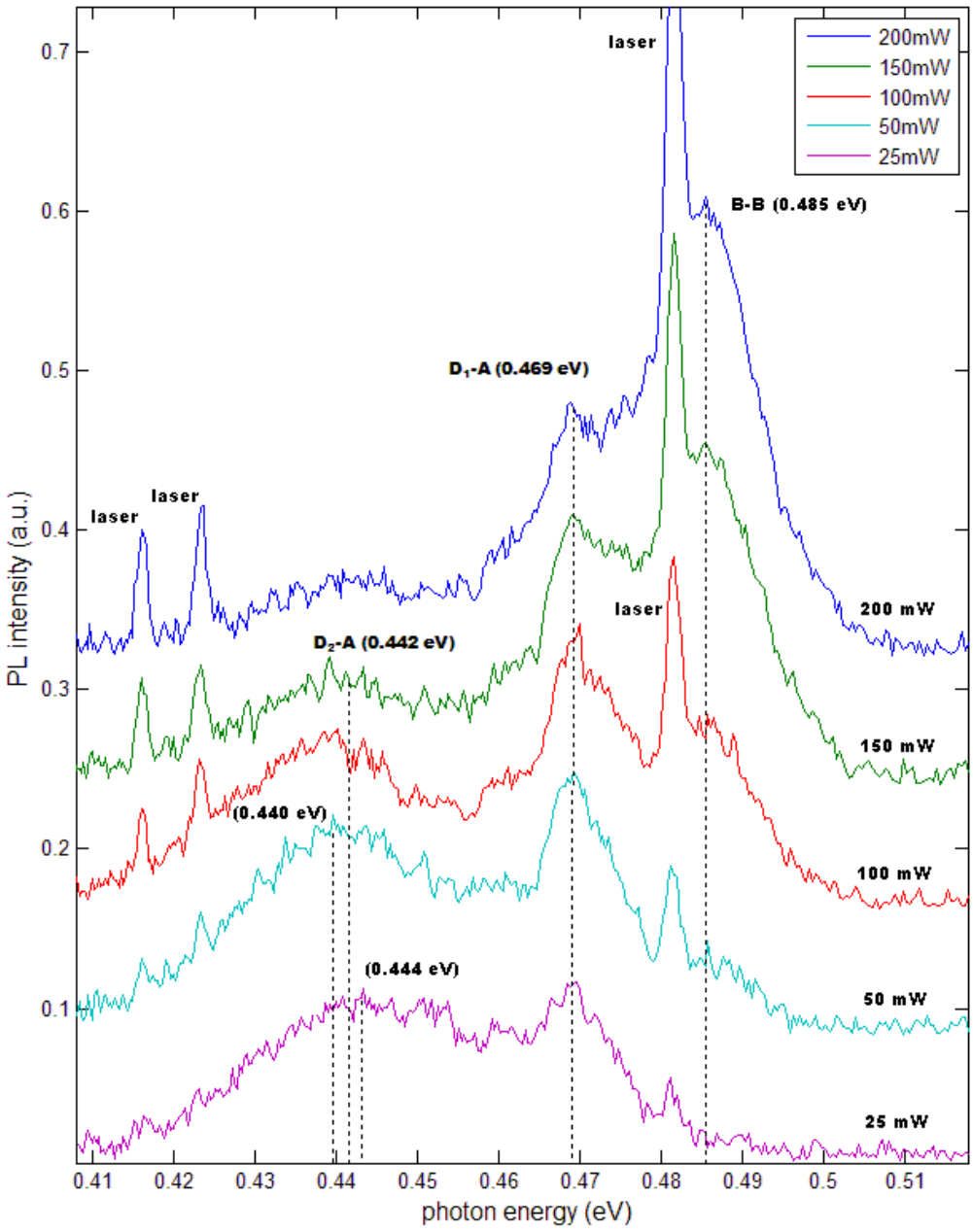

Figure 21. Laser excitation power dependent photoluminescence spectra of $In_{0.93}Ga_{0.07}As$ at 12 K

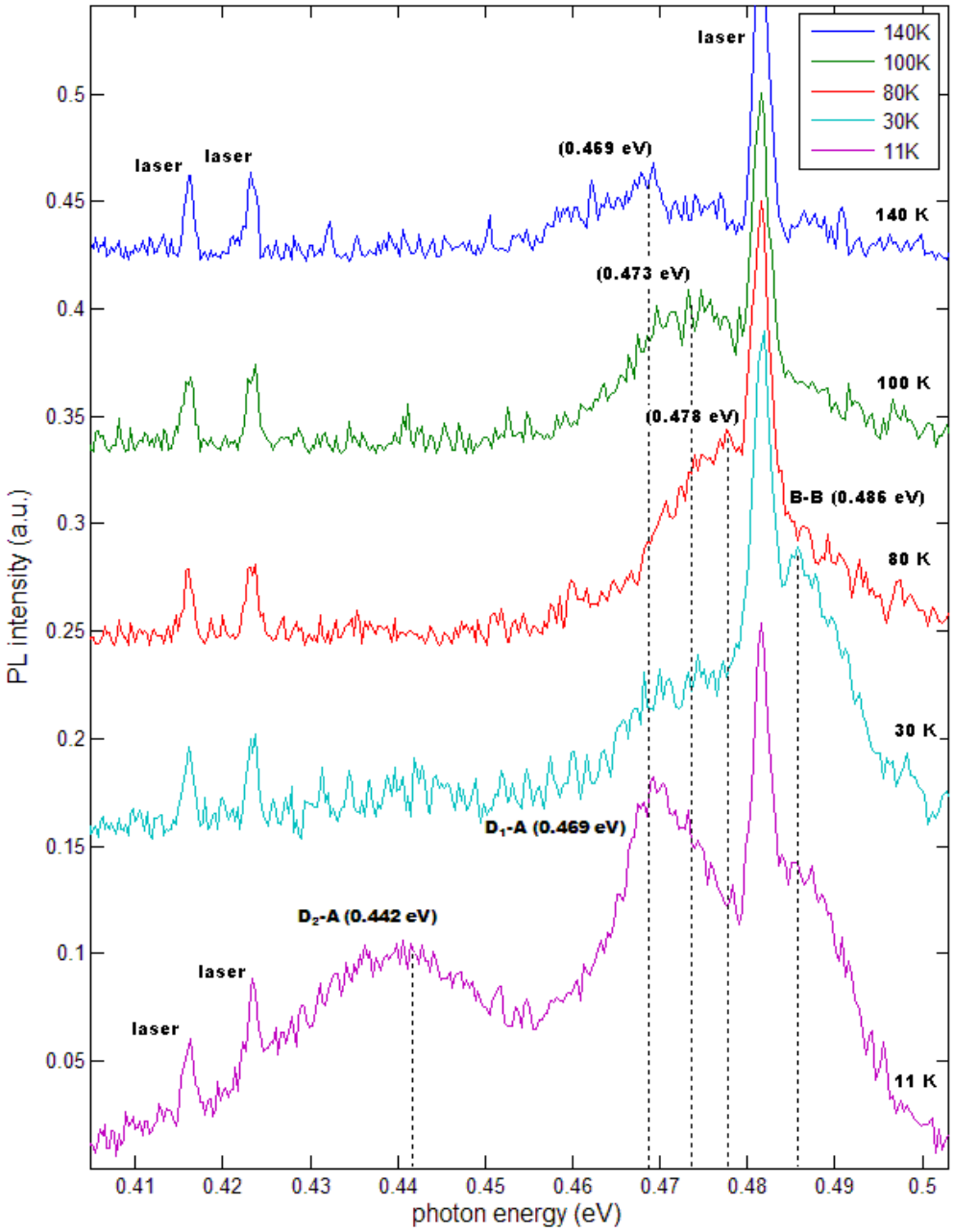

Figure 22. Temperature dependent photoluminescence spectra of $In_{0.93}Ga_{0.07}As$ with 100 mW excitation power.

The highest energy peak at 0.485 eV at 11 K in the power dependent spectra shown in Figure 21, a band-to-band transition, began to appear at 50 mW excitation power and grew monotonically with increasing laser intensity. The peak position for this B-B transition underwent virtually no shift with increasing excitation power, an indication of good thermal contact between the sample and the mount and of good thermal conduction on the part of the sample itself. The second peak due to a shallow donor-acceptor pair transition, located at 0.468 eV at 11 K for all excitation intensities in the power dependent spectra shown in Figure 21, displayed behavior almost identical to that of the peak classified as originating from a donor-acceptor transition in $In_{0.82}Ga_{0.18}As$. This D_1-A peak located at 0.468 eV in power dependent spectra dropped out almost entirely by 40 K in the temperature dependent measurement set and was subsumed by the higher energy band-to-band transition with rising excitation power in the power dependent measurement set. The D_1-A peak's energy separation from the band-to-band transition yielded a 17 meV sum of shallow donor and acceptor ionization energies, a value similar to those measured for $In_{0.75}Ga_{0.25}As$ and $In_{0.82}Ga_{0.18}As$.

The third and lowest energy peak for $In_{0.93}Ga_{0.07}As$, located ambiguously between 0.440 and 0.444 eV in the power dependent spectra displayed in Figure 21, showed strong similarity to the deep donor-acceptor peak in the spectra of $In_{0.75}Ga_{0.25}As$ and the low energy tail seen in the spectra of $In_{0.82}Ga_{0.18}As$. This D_2-A peak's position appeared to decrease in energy as excitation power climbed from 25 to 100 mW, a contradiction of the typical power dependent behavior of donor-acceptor transitions, but it also appeared to increase in energy slightly from the 100 to 200 mW spectra. The 24 – 28 meV

separation between the D_1-A peak and the D_2-A peak points toward a large ionization energy for the deep donor.

Position dependent measurements on this sample (shown in Appendix IV) suggest reasonable uniformity. They displayed no appreciable shift in peak positions, although the relative amplitudes of the peaks were notably different, with the deep donor-acceptor peak disappearing entirely in all but the spectrum used in the above analysis

Results for $In_{0.99}Ga_{0.01}As$ (IGA 061206-6_2)

Hall effect measurements and PL spectroscopy for $In_{0.99}Ga_{0.01}As$ revealed this sample to be the most dissimilar from the others studied here. Temperature dependent Hall mobility results are displayed in Figure 23, and carrier concentration results are displayed in Figure 24. The 10 K carrier concentration was found to be 9.6×10^{16} cm^{-3}. Hall measurement results fluctuated significantly from temperature to temperature, which casts doubt onto individual mobility and carrier concentration values. The mobility, as with other samples, reached a peak at approximately 100 K before dropping with rising temperature, and the jump from low mobility to high at approximately 50 K was remarkably abrupt, likely reflecting a measurement anomaly rather than interesting physics connected to the sample itself. Carrier concentrations fluctuated significantly and appeared to drop in the mid temperature range, reaching their minimum between 50 and 100 K, similar to the carrier concentration of $In_{0.93}Ga_{0.07}As$, $In_{0.91}Ga_{0.09}As$, and InAs (which is discussed in the following section). But the carrier concentration did, like the carrier concentrations in other samples, remain essentially flat until beginning to rise significantly between 50 and 100 K due to deep donor carriers.

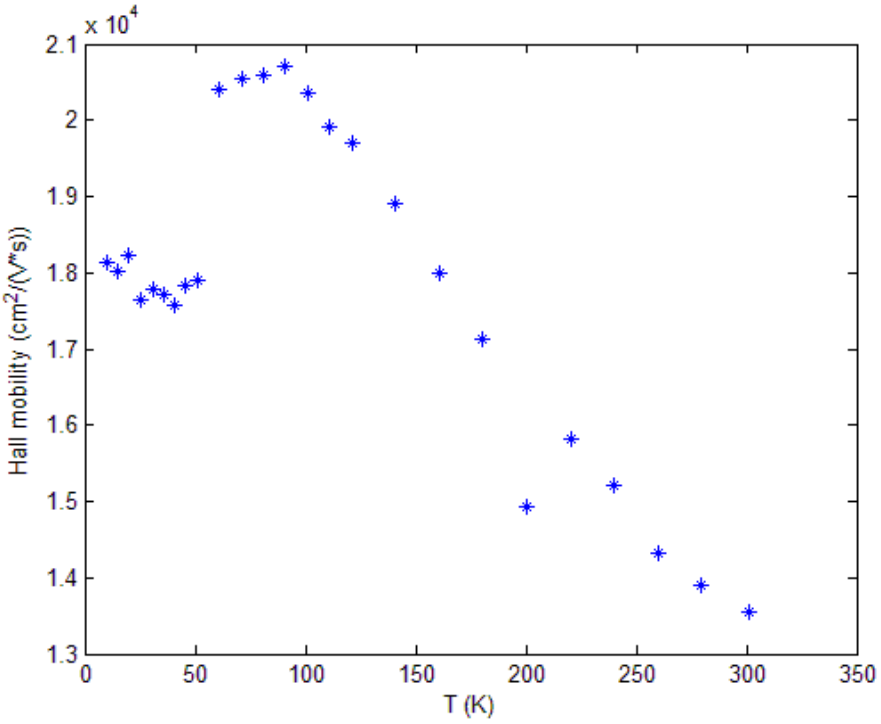

Figure 23. Temperature dependent Hall mobility of $In_{0.99}Ga_{0.01}As$

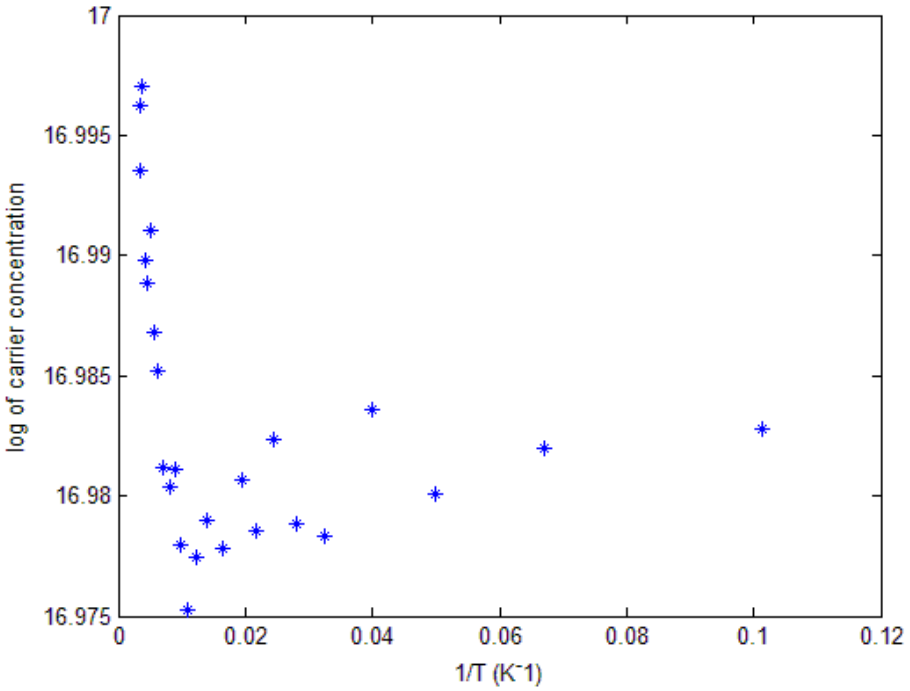

Figure 24. Log of carrier concentration vs. inverse temperature for $In_{0.99}Ga_{0.01}As$

PL spectra for this sample (Figure 25, Figure 26, and Appendix V) reveal a single, broad peak with a stable, low-energy tail. Figure 25 shows laser excitation power dependent spectra at 12 K, and Figure 26 displays temperature dependent PL spectra under 200 mW laser excitation for temperatures ranging from 12 to 70 K. Based on the high carrier concentration found in the Hall effect measurements, the large, low energy tail on the peak likely arose due to band-tailing, a phenomenon in which the donor levels merge with the conduction band once a threshold doping level has been reached. These donor levels then form a continuum of states extending below the fundamental, undoped band gap energy of the sample. The tail of states on this peak (classified as a band-to-band transition) persisted through all temperature dependent measurements, suggesting the continuity of these states with the rest of those contributing to the transition. And as with the other samples studied here, the transition dropped toward lower energy with increasing temperature, illustrated in the temperature dependent PL spectra displayed in Figure 26.

Position dependent measurements (shown in Appendix V) suggest a poor quality sample, and peak positions and PL intensity vary greatly across the sample. The variation in peak position points to a 0.5-percent variation in indium content across the sample. And in taking PL measurements, it was difficult to find positions with strong emission, heuristically supporting the case for poor sample quality and non-uniform sample composition.

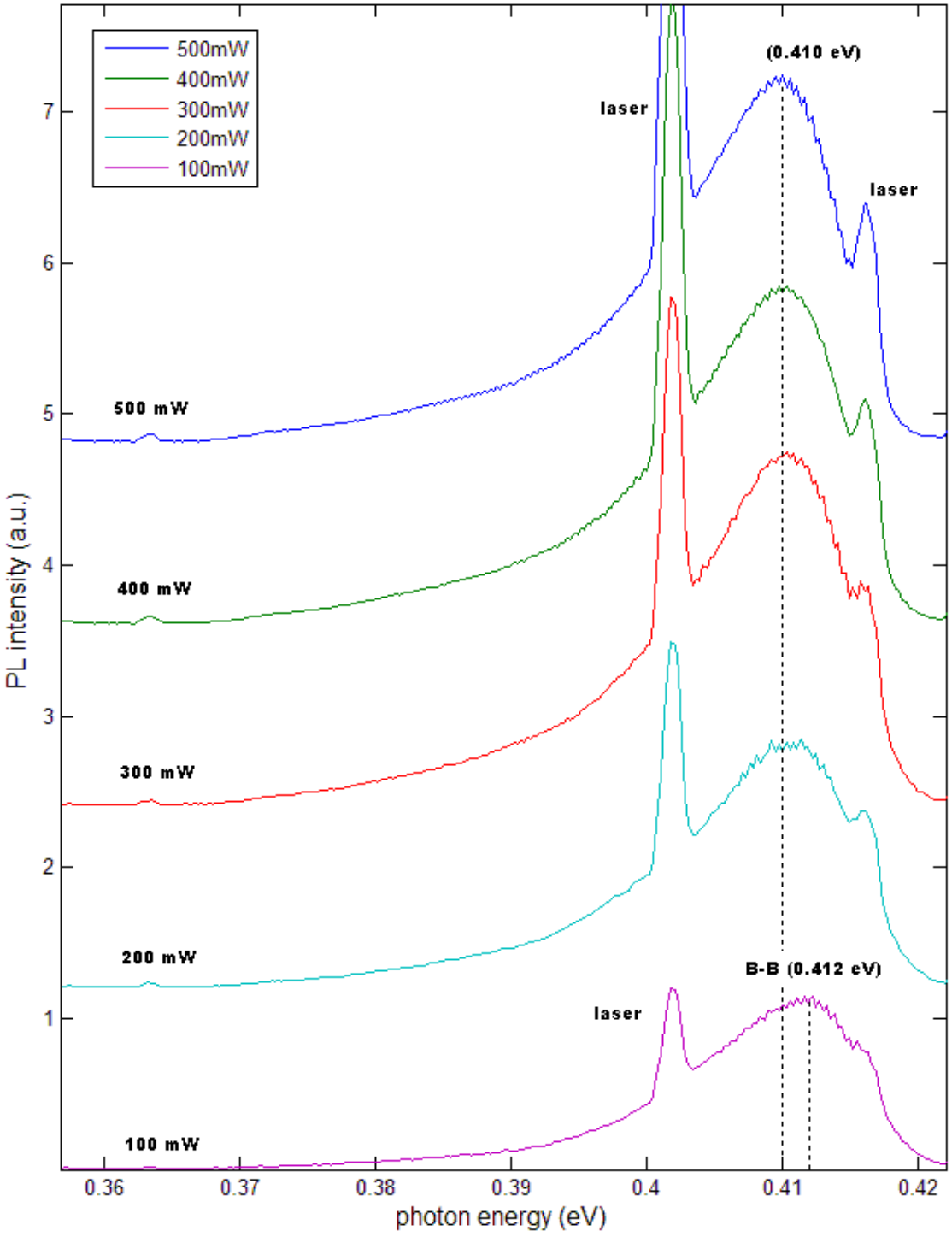

Figure 25. Laser excitation power dependent photoluminescence spectra for $In_{0.99}Ga_{0.01}As$ at 12 K

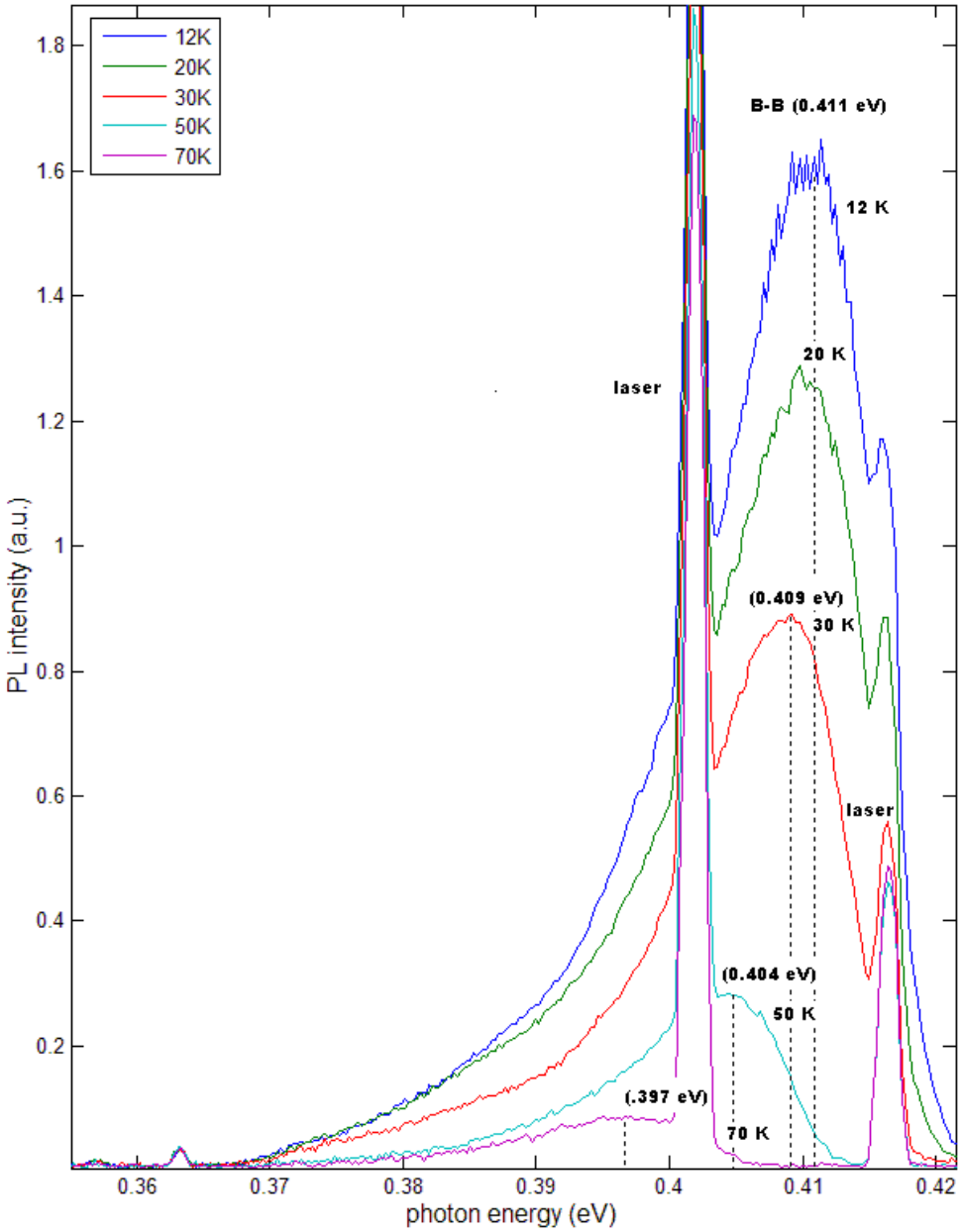

Figure 26. Temperature dependent photoluminescence spectra of $In_{0.99}Ga_{0.01}As$ with 200 mW excitation power

Results for InAs

InAs displayed perhaps the most typical Hall effect data and the most unique PL data of the samples studied. As with other samples, InAs displayed Hall mobility increasing until approximately 100 K at which point optical phonon scattering took effect and drove down carrier mobility, as pictured in Figure 27. The significant jump by a factor of two in mobility from $In_{0.99}Ga_{0.01}As$ to InAs (1.8×10^4 $cm^2/V\cdot s$ for $In_{0.99}Ga_{0.01}As$ to 3.5×10^4 $cm^2/V\cdot s$ for InAs at 10 K) likely occurred because of the disappearance of alloy scattering as a mobility inhibitor in addition to decrease in defect and impurity scattering due to the ease associated with InAs growth compared to the growth of ternary alloys.

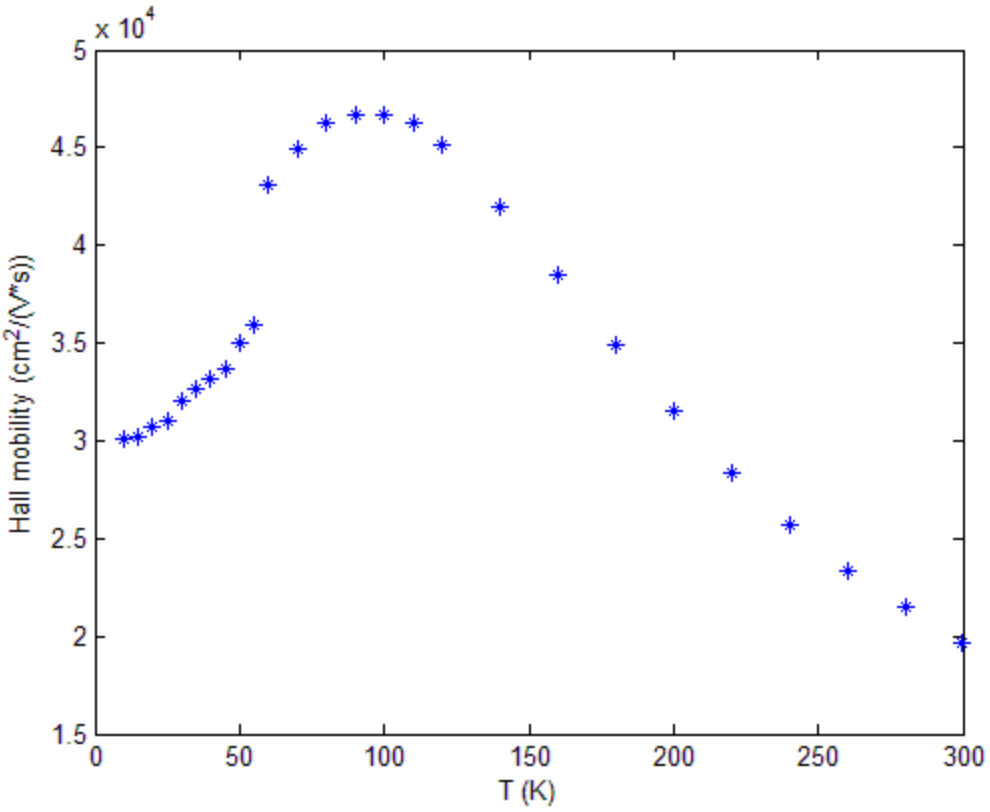

Figure 27. Temperature dependent Hall mobility of InAs

The carrier concentration measurements, depicted in Figure 28 below, displayed behavior similar to that of the other samples studied. A slight drop in carrier concentration appeared to occur between 25 and 80 K, and in this case the measurement set was free of unexplained fluctuations in carrier concentrations between adjacent temperatures, which suggests a legitimate reason for the apparent decrease in carrier concentration.

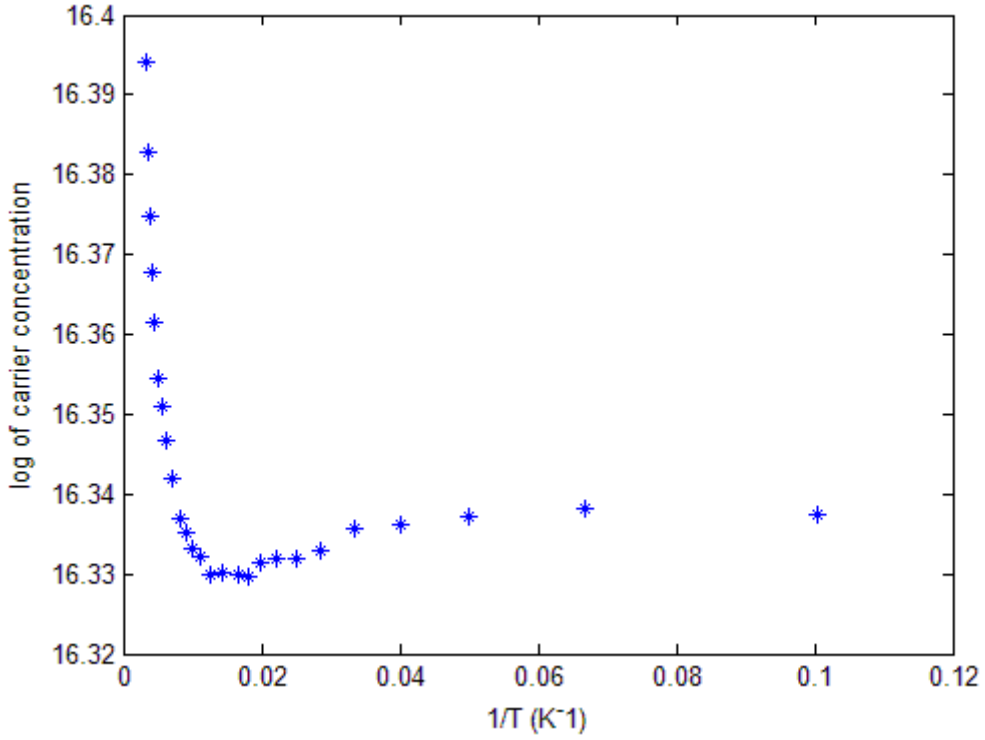

Figure 28. Log of carrier concentration vs. inverse temperature for InAs

The PL spectra for InAs were the most unique compared to the other samples analyzed. Figure 29 displays laser excitation power dependent PL spectra at 12 K, and Figure 30 displays temperature dependent PL spectra under 300 mW laser excitation power. The 100 mW spectrum shown in Figure 29 displayed a sharp narrow peak at

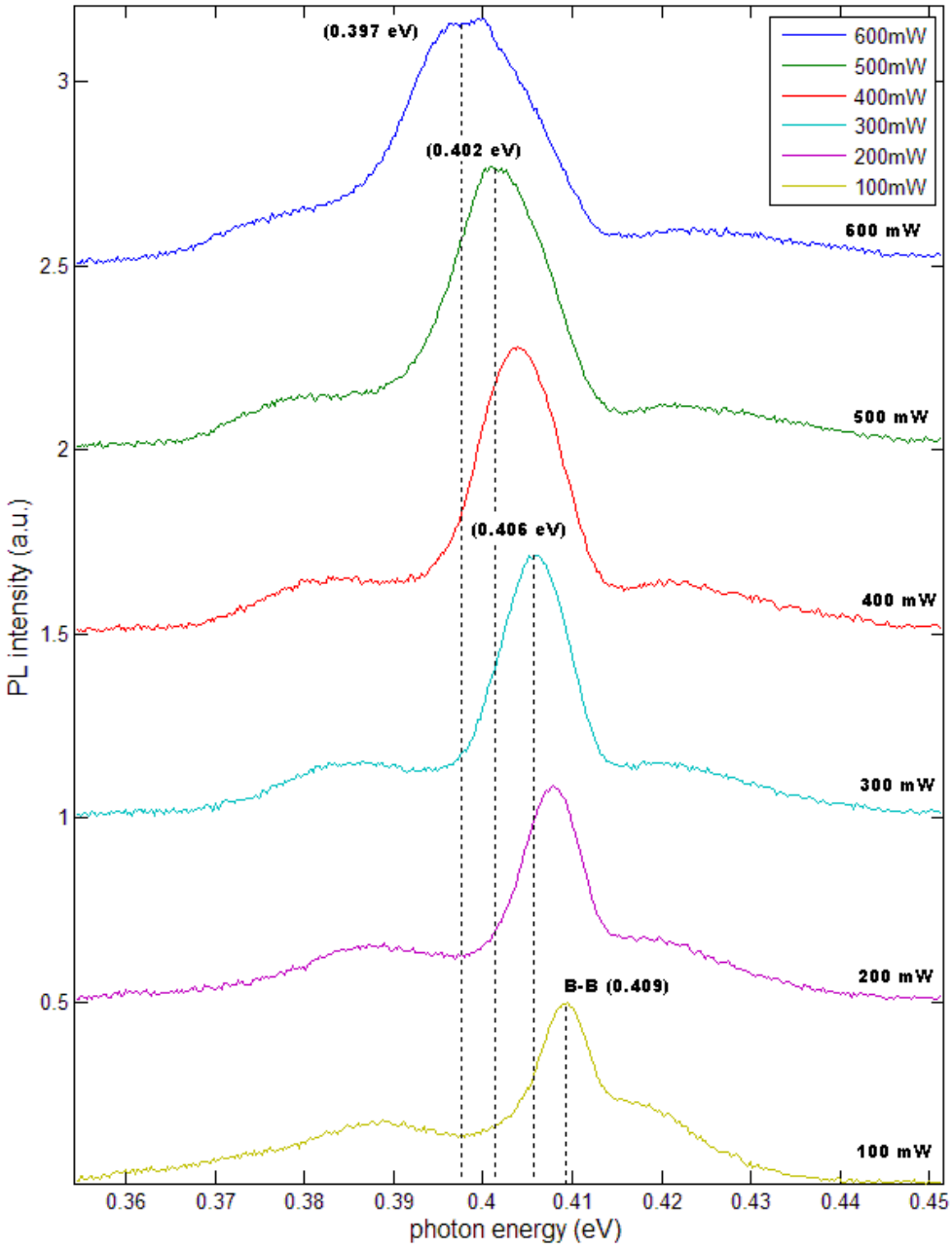

Figure 29. Laser excitation power dependent photoluminescence spectra of InAs at 12 K

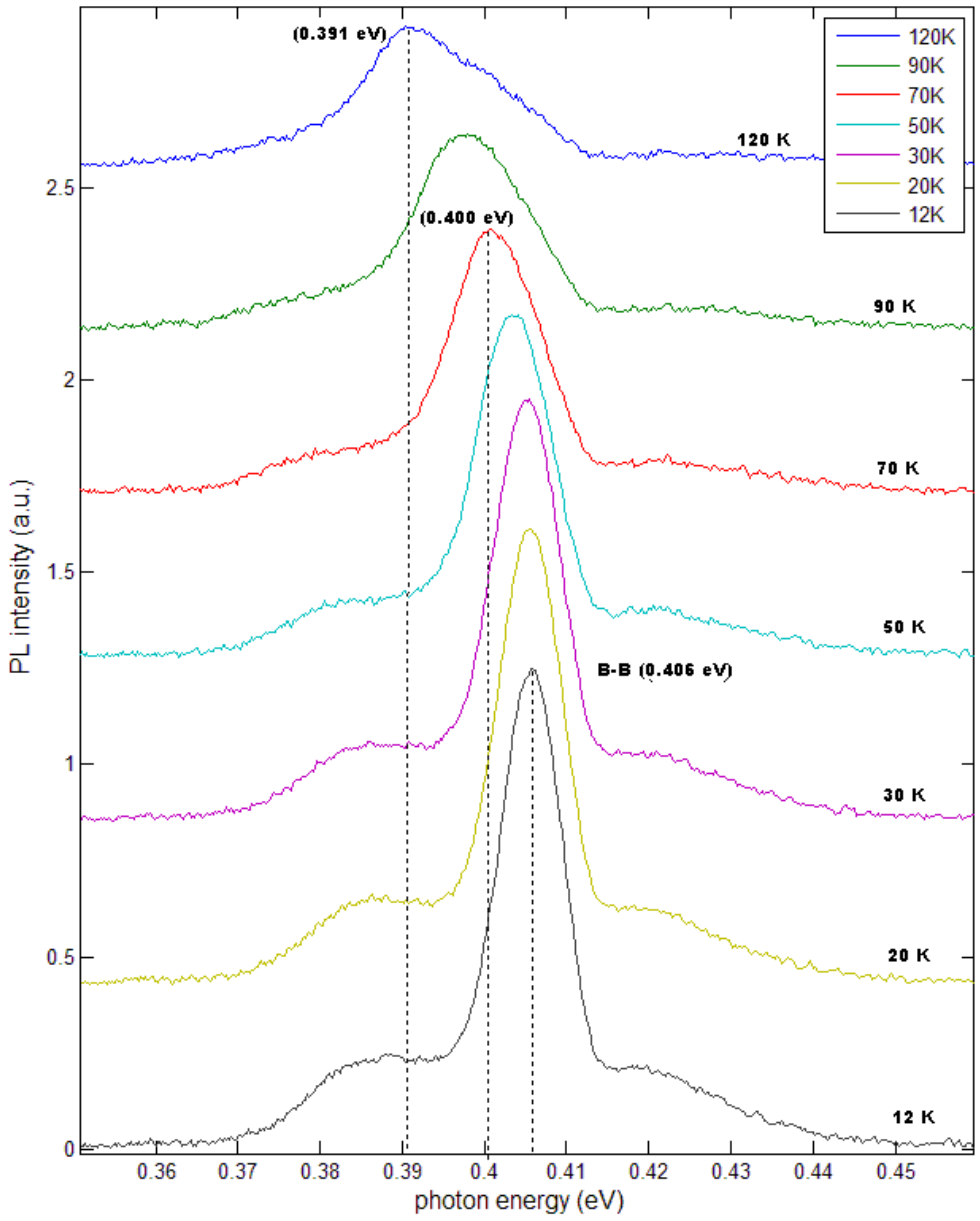

Figure 30. Temperature dependent photoluminescence spectra for InAs with 300 mW excitation power

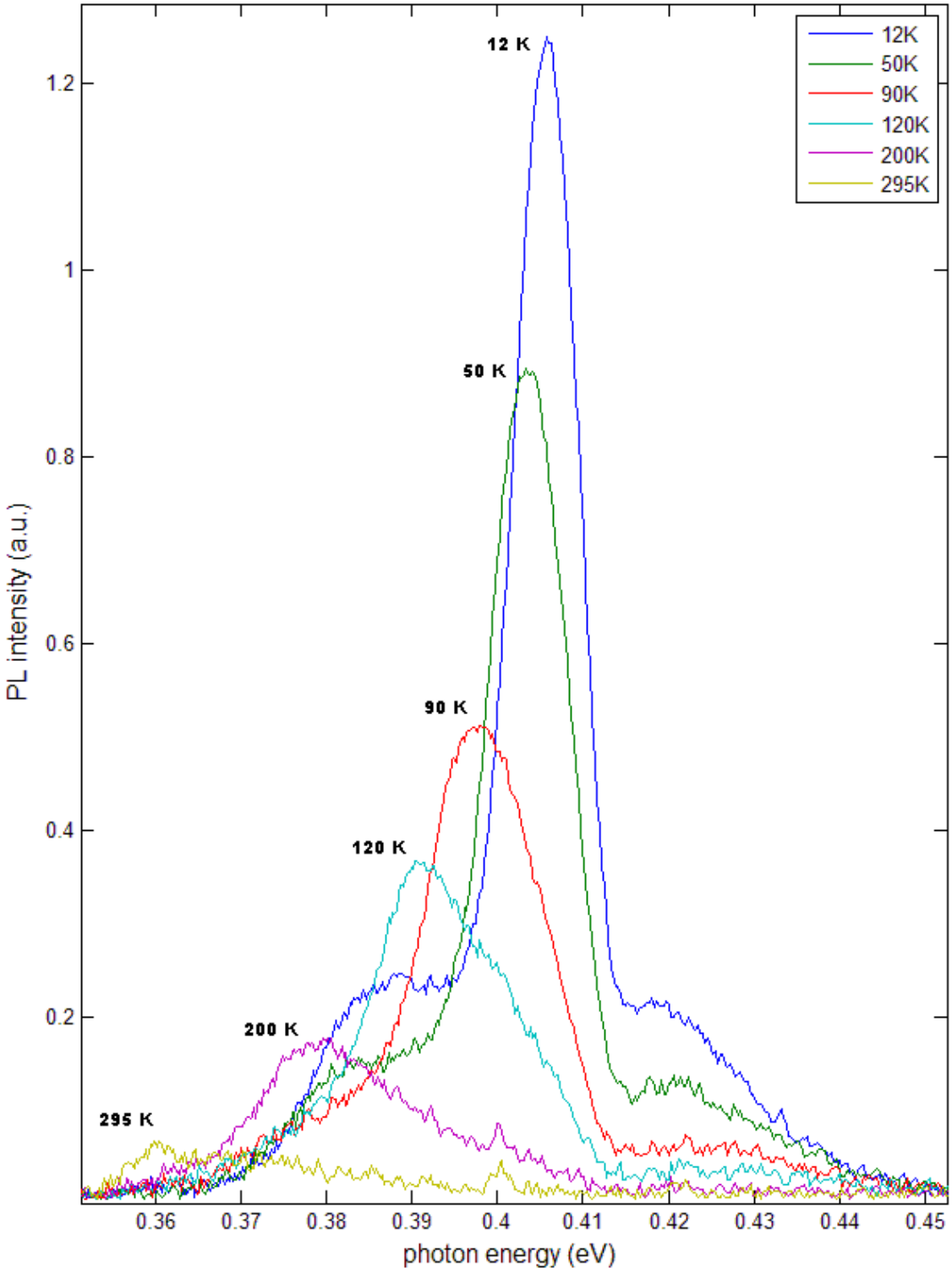

Figure 31. Temperature dependent photoluminescence spectra for InAs with 300 mW excitation power

approximately 0.410 eV with a pedestal extending approximately 25 meV toward higher energies and 40 meV toward lower energies. With rising temperatures, as shown in the temperature dependent spectra of Figure 30, this sharp peak occurring at 0.410 eV under 100 mW excitation power at 12 K would eventually take the classic band-to-band form in which intensity rises sharply and then tapers off with a Maxwellian tail at higher energies. In this case, the low energy shoulder is believed to be due to a donor-acceptor pair transition, and the high energy shoulder peak associated with the band-to-band transition is believed to result from a non-parabolicity in the conduction band generating an unusual density of states. Additionally, self-absorption, not otherwise considered in this study due to a lack of detailed absorption data and information about the depth of laser penetration, may play a role in the unusual shape. Despite the complexity displayed, because of the tall, narrow peak's uncannily strong resemblance to a band-to-band transition at high temperatures, it is believed that this peak does not arise from an impurity related mechanism or excitonic transition but from a band-to-band transition.

Summary

The data for the set of samples considered showed consistency both through the Hall effect measurements and PL spectra. The samples studied exhibited varied quality, some displaying low carrier concentrations and good uniformity, others having high impurity content and widely varied composition. Band gaps and mobilities varied as expected with crystal composition. Hall effect measurements corroborated and explained the results of PL measurements, helping to explain the varied features seen among the spectra of the various samples.

V. Conclusions and Recommendations

Chapter Overview

This section summarizes the findings of the study and examines their significance. It works to create coherent picture of the research that has taken place and its meaning.

Conclusions of Research

The samples studied exhibited varied quality. Some samples showed clear variation in composition based on PL peak positions, and those that did not show this variation in peak position had varied PL intensities with position, suggesting non-uniform quality. Impurity concentrations were not constant from sample to sample but changed by approximately a factor of five across the set, suggesting at least a mild inability to control incorporation of impurities during growth. Based on the criteria of P.S. Dutta outlined in the introduction to this study [1], the samples considered here are likely not yet in a state to be useful as substrates for high quality semiconductor devices. In comparison to on other research performed, particularly at Fujitsu Laboratories, the Vertical Bridgman-grown samples here do not meet the standards for crystal quality attained by other researchers. There is not, however, a major body of work relating to optical and electrical characterization of bulk $In_xGa_{1-x}As$ alloys. Most of the characterization research (aside from x-ray diffraction and similar techniques) has focused on epitaxial layers nearing device quality rather than on their substrates. Accordingly, these samples and their characterization may contribute to the body of knowledge on the bulk ternary alloy $In_xGa_{1-x}As$.

Recommendations for Future Research

Future research should focus on both the improvement of crystal quality and on achieving higher fidelity in characterization work. High temperature Hall measurements, performed with properly evaporated contacts capable of achieving temperatures on the order of 700 – 800 K, could allow determination of band gap based on the growth of intrinsic carrier concentrations with increasing temperature. Thinner samples used in Hall effect measurements could be used to achieve greater accuracy with the van der Pauw method. Liquid helium immersion could allow better temperature control, opening up thus far unexamined optical transitions in bulk alloys for comparison with their epitaxial counterparts.

Beyond extending work with characterization techniques used here, techniques such as X-ray fluorescence, scanning electron microscopy, and atomic force microscopy could also be used to gauge sample quality and offer greater fundamental understanding. X-ray fluorescence could be used to determine the donor and acceptor species present in the samples. This knowledge might then be used by the crystal grower to determine the source of the impurity species and limit their presence in the melt. Scanning electron microscopy and atomic force microscopy could offer a precise picture of surface level defects and determine the presence of cracks and polycrystallinity. Knowing the nature of defects would allow the crystal grower insights on how to best proceed with subsequent growth work.

Appendix I: Additional Photoluminescence Spectra for $In_{0.75}Ga_{0.025}As$

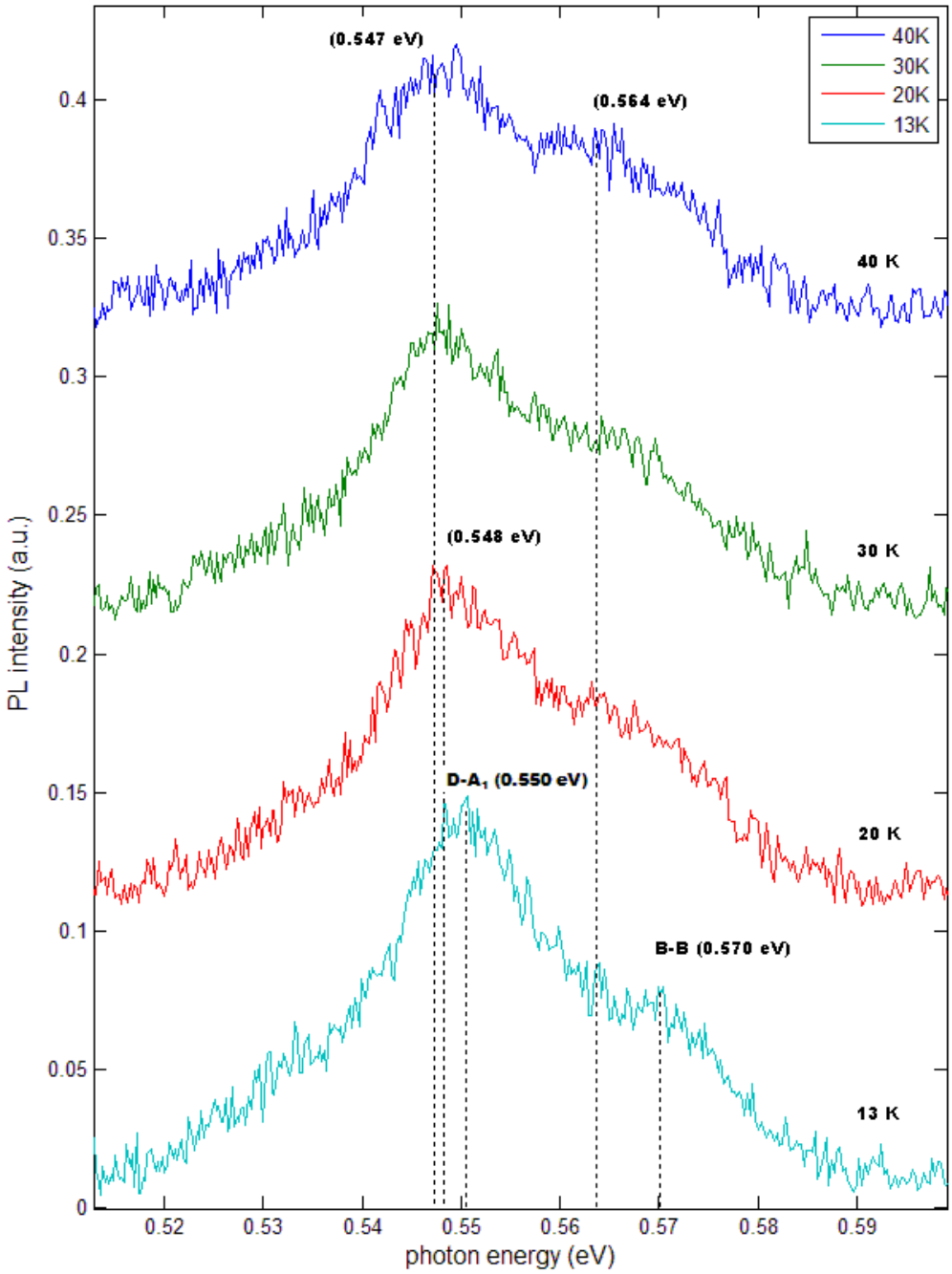

Figure 32. Temperature dependent photoluminescence spectra of $In_{0.75}Ga_{0.025}As$ with 200 mW excitation power

Appendix II: Additional Photoluminescence Spectra for $In_{0.82}Ga_{0.18}As$

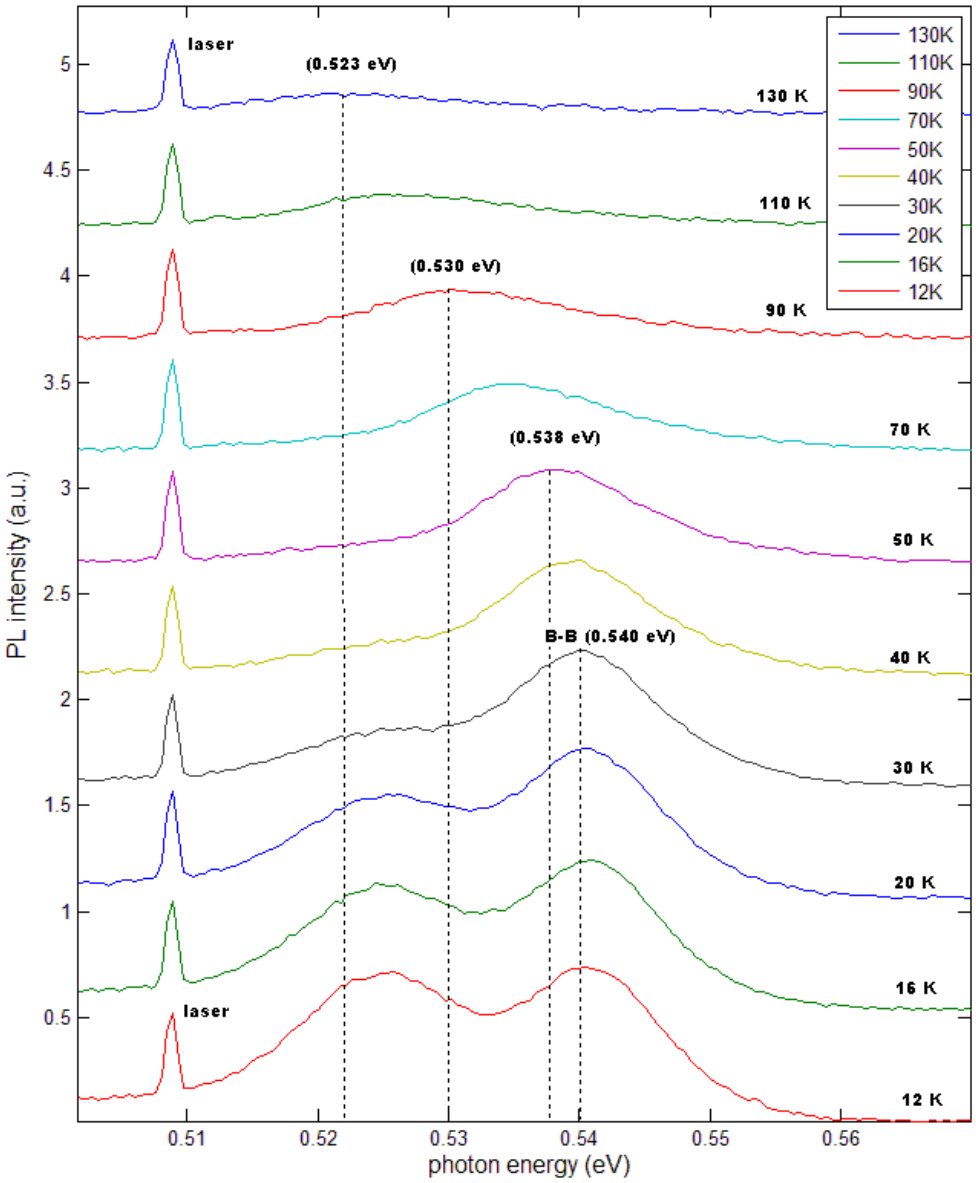

Figure 33. Temperature dependent PL spectra of $In_{0.82}Ga_{0.18}As$ with 400 mW excitation power

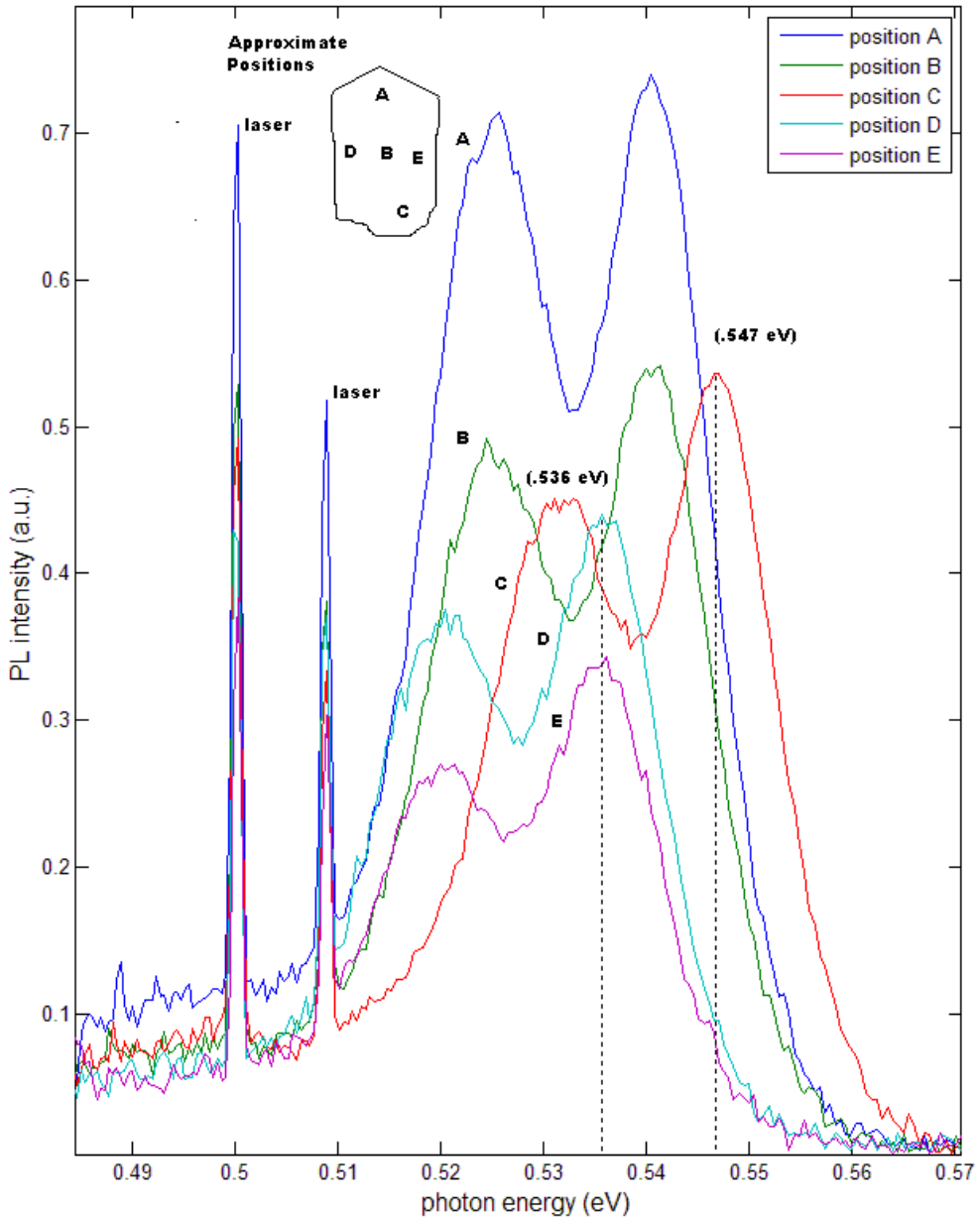

Figure 34. Position dependent PL spectra of $In_{0.82}Ga_{0.18}As$ at 12 K with 400 mW excitation power

Appendix III: Additional Photoluminescence Spectra for $In_{0.91}Ga_{0.09}As$

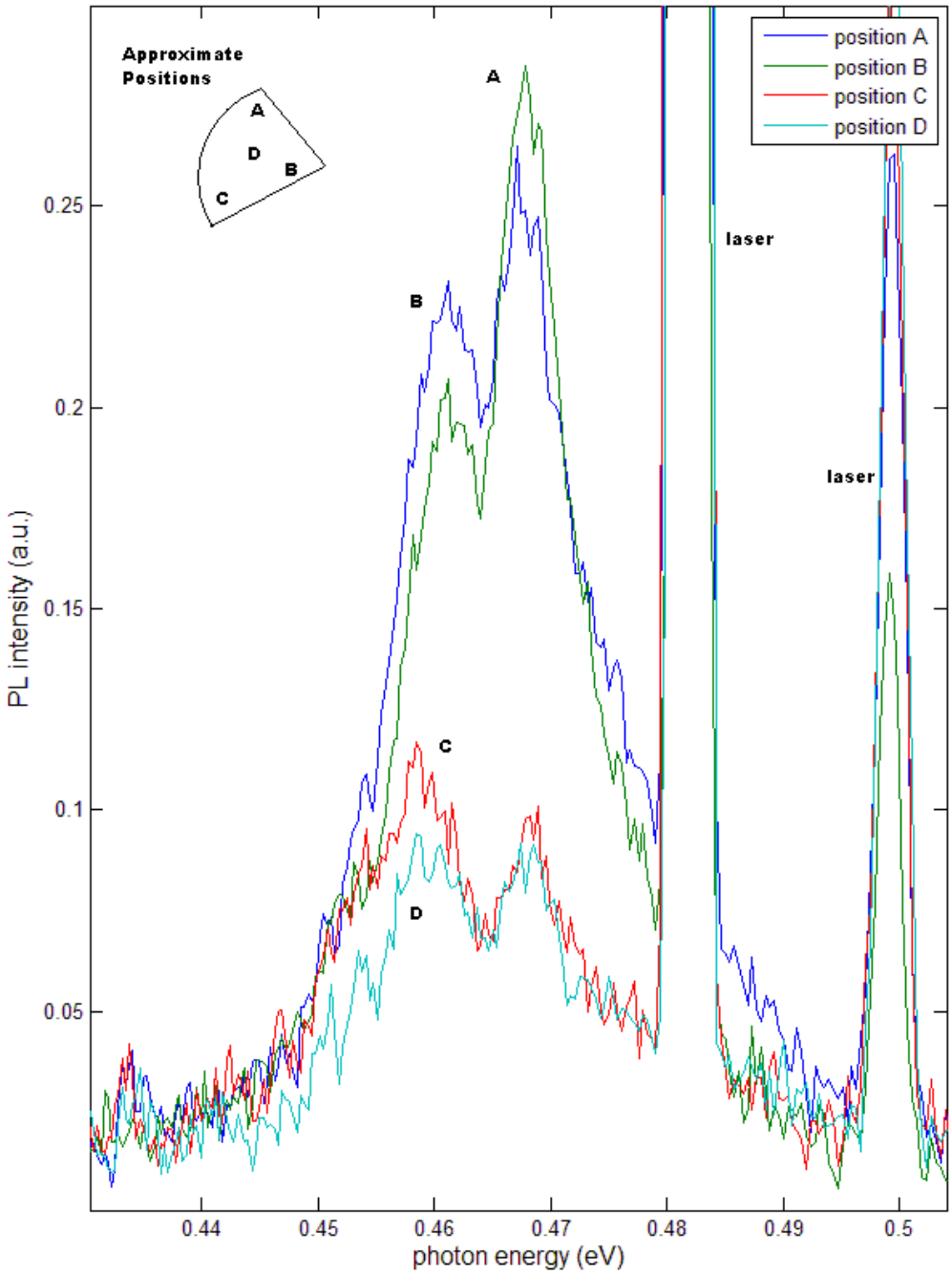

Figure 35. Position dependent photoluminescence spectra of $In_{0.91}Ga_{0.09}As$ at 12 K with 350 mW excitation power

Appendix IV: Additional Photoluminescence Spectra for $In_{0.93}Ga_{0.07}As$

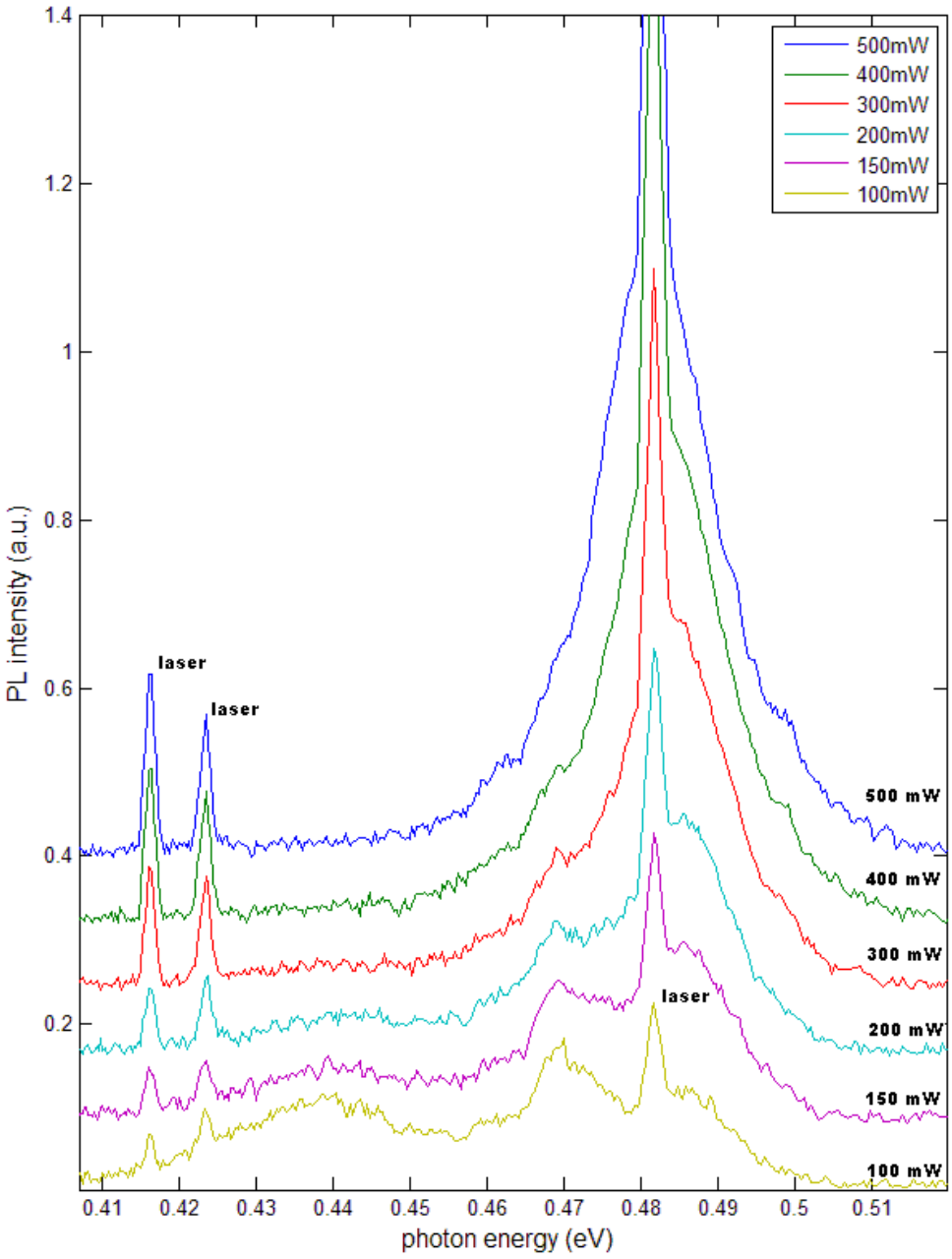

Figure 36. Power dependent photoluminescence spectra of $In_{0.93}Ga_{0.07}As$ at 12 K

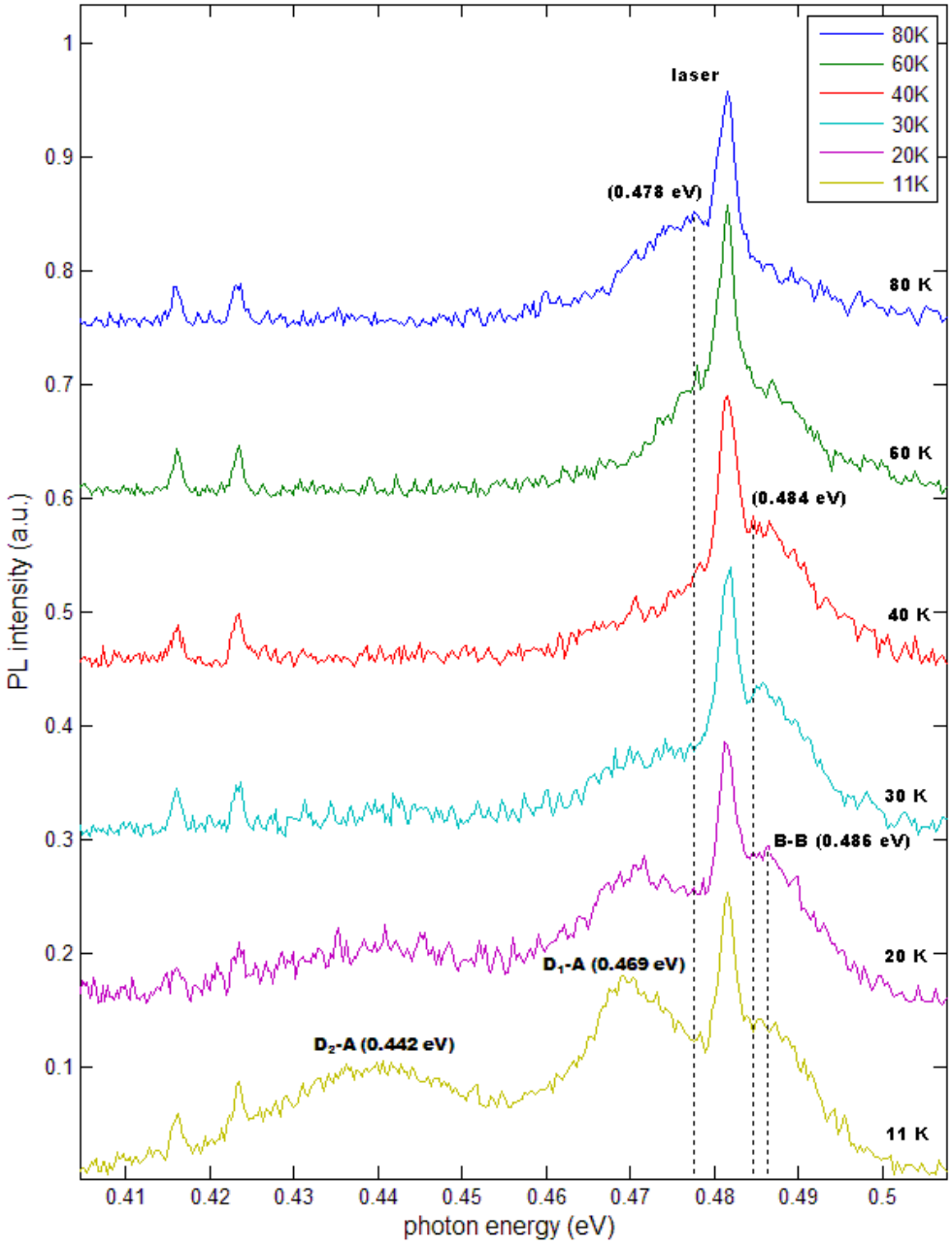

Figure 37. Temperature dependent photoluminescence spectra of $In_{0.93}Ga_{0.07}As$ with 100 mW excitation power

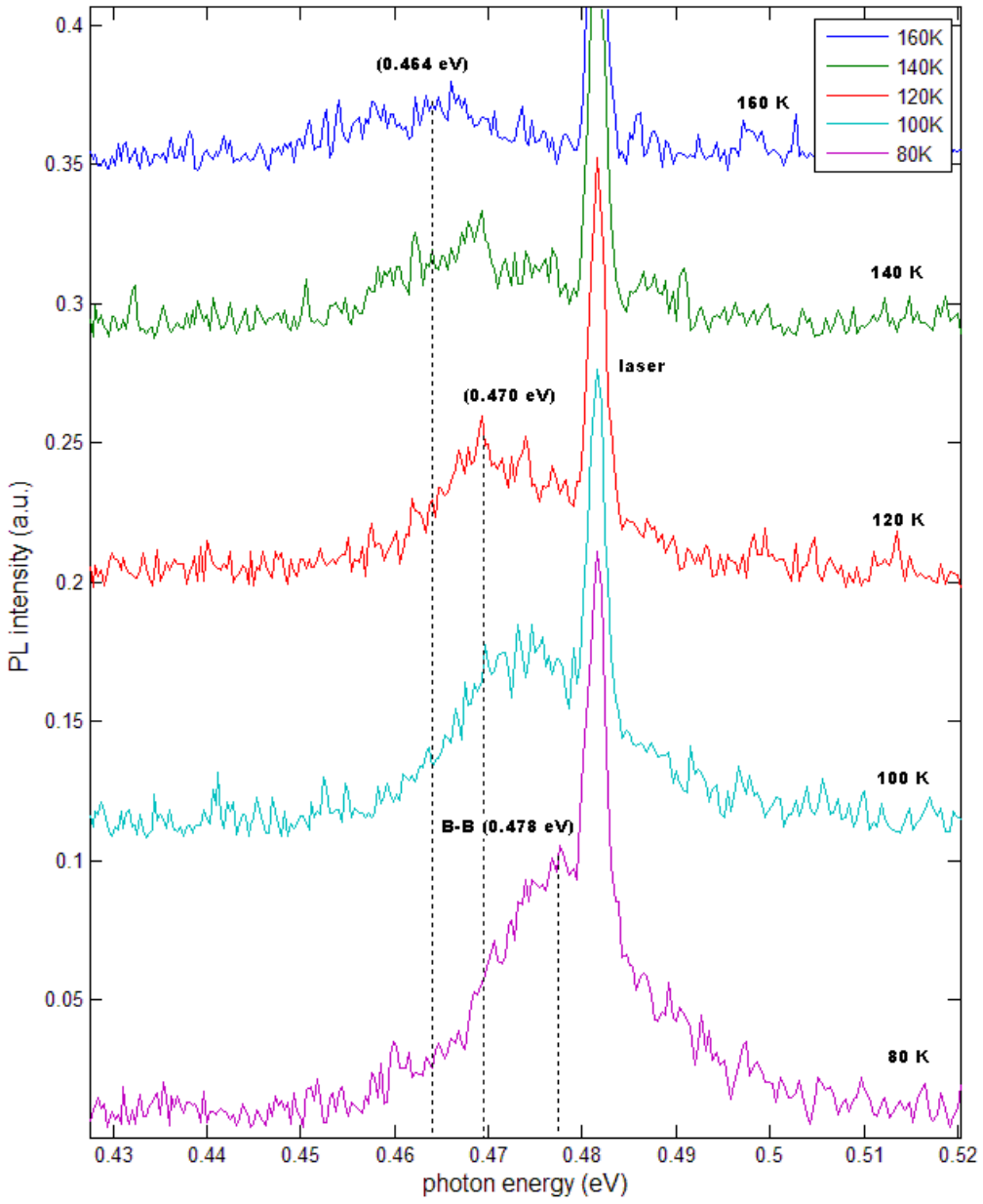

Figure 38. Temperature dependent photoluminescence spectra of $In_{0.93}Ga_{0.07}As$ with 100 mW excitation power

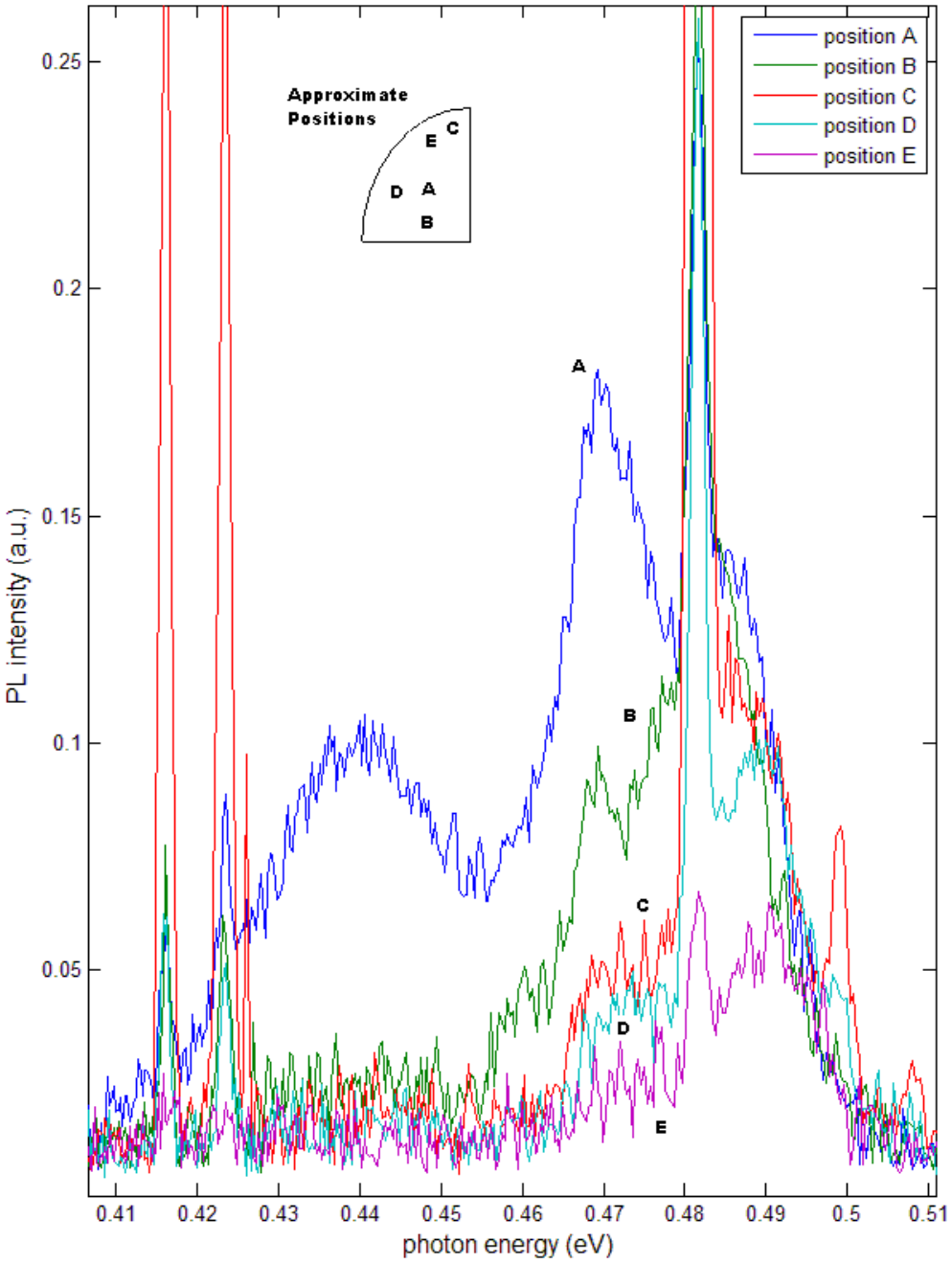

Figure 39. Position dependent photoluminescence spectra of $In_{0.93}Ga_{0.07}As$ at 12 K with 100 mW excitation power

Appendix V: Additional Photoluminescence Data for $In_{0.99}Ga_{0.01}As$

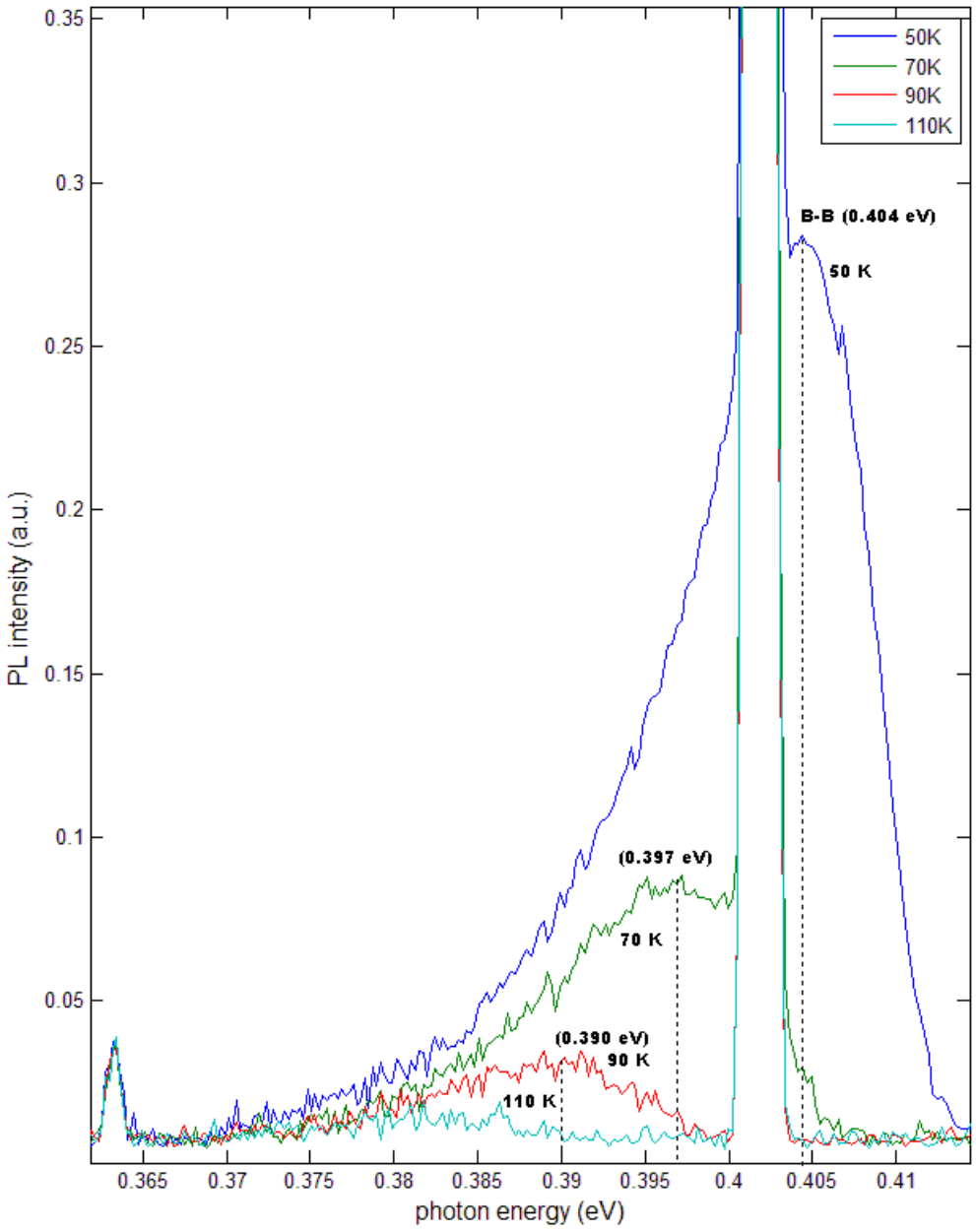

Figure 40. Temperature dependent photoluminescence spectra of $In_{0.99}Ga_{0.01}As$, 50 with 200 mW excitation power

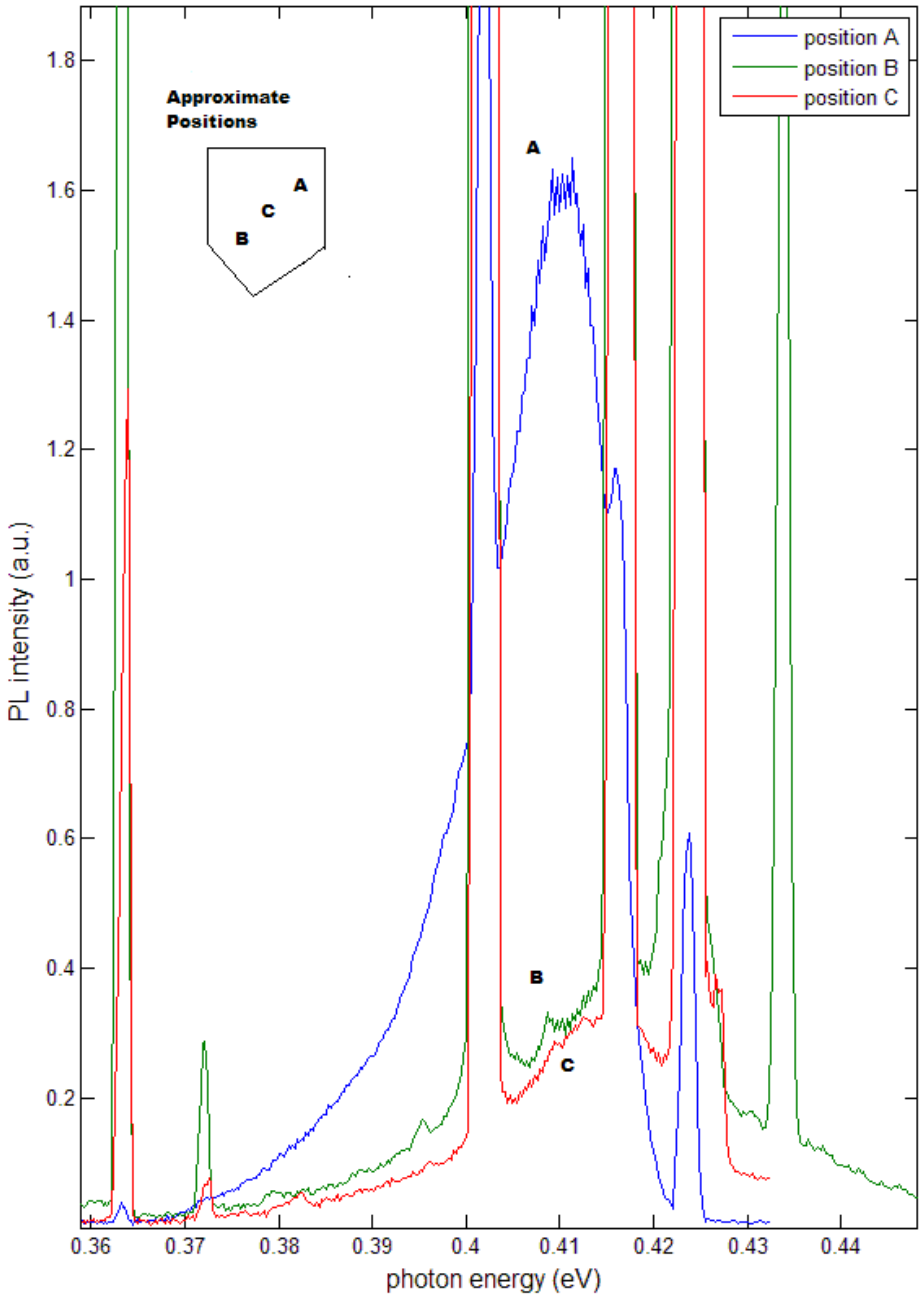

Figure 41. Position dependent photoluminescence spectra of $In_{0.99}Ga_{0.01}As$ at 12 K with 200 mW excitation power

Appendix VI: Additional Photoluminescence Spectra for InAs

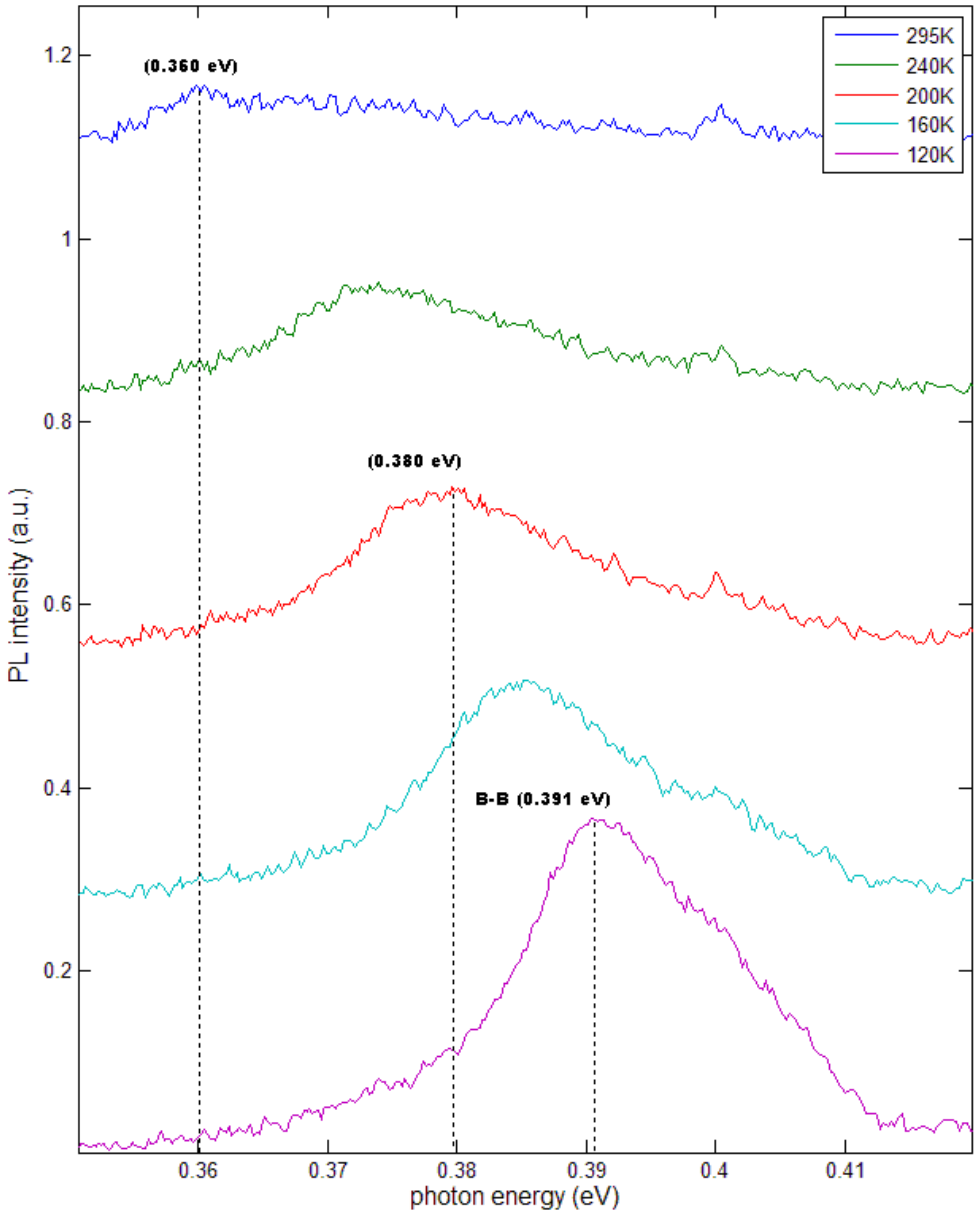

Figure 42. Temperature dependent photoluminescence data of InAs with 300 mW excitation power

Bibliography

1. Dutta, P. S. "III-V Ternary bulk substrate growth technology: a review." *Journal of Crystal Growth.* vol. 275, pp. 106-112, 2005.

2. Islam, M.R., P. Verma, and M. Yamada. "Study on polycrystallization in bulk $In_xGa_{1-x}As$ using micro-Raman and photoluminescence." *Journal of Crystal Growth*. vol. 263, pp. 125-131, 2004.

3. Kusunoki, Toshihiro, Chisato Takenaka, and Kazuo Nakajima. "LEC growth of InGaAs bulk crystal fed with a GaAs source." *Journal of Crystal Growth.* vol. 112, pp. 33-38, 1991.

4. Ozawa, T., Y. Hayakama, K. Balakrishnan, F. Ohonishi, T. Koyama, and M. Kumagawa. "Growth of $In_xGa_{1-x}As$ bulk mixed crystals with a uniform composition by the rotational Bridgman method." *Journal of Crystal Growth.* vol. 229, pp. 124-129, 2001.

5. Nishijima, Yoshito, Kazuo Nakajima, Koji Otsubo, and Hiroshi Ishikawa. "InGaAs single crystal with a uniform composition in the growth direction grown on an InGaAs seed using the multicomponent zone growth method." *Journal of Crystal Growth*. vol. 208, pp. 171-178, 2000.

6. Nishijima, Yoshito, Hiroshige Tezuka, and Kazuo Nakajima. "A modified zone growth method for an InGaAs single crystal." *Journal of Crystal Growth.* vol. 280, pp. 364-371, 2005.

7. Nishijima, Yoshito, Koji Otsubo, Hiroshige Tezuka, Kazuo Nakajima, Hiroshi Ishikawa. "InGaAs zone growth single crystal with convex solid-liquid interface toward the melt." *Journal of Crystal Growth*. vol. 245, pp. 228-236, 2002.

8. Kodoma, Shigeo, Yuji Furumura, Kyoichi Kinoshita, Hirokazu Kato, and Shinichi Yoda. "Single crystalline growth of $In_{0.3}Ga_{0.7}As$ on GaAs seed using the multi-component zone melting method." *Journal of Crystal Growth.* vol. 208, pp. 165-180, 2000.

9. Suzuki, T., T. Kusunoki, and K. Nakajima. "Multicomponent Zone Melting Growth of Ternary InGaAs Bulk Crystal." Conference Proceedings, 7th Annual Conference on Indium Phosphide and Related Materials. pp. 45-48, 1995.

10. Fellows, J. "Electrical Activation Studies of Ion Implanted Gallium Nitride," Ph.D. dissertation, Air Force Institute of Technology (AU), Wright-Patterson AFB OH, 2001.

11. M. Fox. *Optical Properties of Solids*. Oxford University Press, 2001.

11. Pankove, Jacques. *Optical Processes in Semiconductors.* Dover Publications, Inc., 1970.

13. J. McKelvey. *Solid State Physics for Engineering and Materials Science*. Krieger Publishing Compary, 1993.

14. Ansara, Ibrahim *et al.*. "Arsenic – Gallium – Indium." Landolt-Bornstein Numerical data and functional relationships in science and technology. vol. 2. Ternary Alloy Systems: Phase Diagrams, Crystallographic and Thermodynamic Data. Ed. W. Martienssen. pp. 159 – 177.

15. Wu, T. Y., and G. L. Peterson. "Phase Diagram, Crystal Growth, and Band Structure of $In_xGa_{1-x}As$." Journal of Physics and Chemistry of Solids. vol. 33. pp. 409-415, 1971.

16. Vurgaftman, I., J.R. Meyer, and L.R. Ram-Mohan. "Band parameters for III-V semiconductors and their alloys." *Journal of Applied Physics.* vol. 89, pp. 5839-5840. 2001.

17. Nakajima, Kuzuo and Toshiro Kusunoki. "Constant temperature LEC growth of InGaAs ternary bulk crystals using the double crucible method." *Journal of Crystal Growth.* vol. 169, pp. 217-222, 1996.

18. Nishijima, Yoshito, Kazuo Nakajima, Koji Otsubo, and Hiroshi Ishikawa. "InGaAs single crystal growth using a GaAs seed grown with the vertical gradient freeze technique." *Journal of Crystal Growth*. vol. 197, pp. 769-776, 1999.

19. Hayakawa, Y., T. Ozawa, T. Azaraki, M. Haris, and M. Kumagawa."Growth of InGaAs ternary bulk crystals by rotational Bridgeman method." *Journal of Crystal Growth*. vol. 275, pp. e421-e425, 2005.

20. Soldatenkov, F. Yu., V. P. Ulin, A. A. Yakovenko, O. M. Fedorova, S. G. Konnikov, and V. I. Korol'kov. "Unstrained epitaxial $In_xGa_{1-x}As$ films obtained on porous GaAs." Technical Physics Letters. vol. 25. pp. 852-854, 1999.

21. Buckley, D. N. "Growth of InGaAs in a hot-walled vapor phase epitaxy reactor using a trimethylarsenic source." Applied Physics Letters. vol. 55, pp. 2514-2516, 1989.

22. Abdalla, M. I., D. G. Kenneson, W. Powazinik, and E. S. Koteles. “Metalorganic vapor phase epitaxial growth of high quality InGaAs on InP using tertiarybutylarsine.” Applied Physics Letters. vol. 57, pp. 494-496, 1990.

23. Keiper, D., R. Westphalen, G. Landgren. “Metal organic vapour-phase epitaxy (MOVPE) growth of InP and InGaAs using tertiarybutylarsine (TBA) and tertiarybutylphosphine (TBP) in N_2 ambient.” Journal of Crystal Growth. vol. 204, pp. 256-262, 1999.

24. Oe, Kunishige. “Low-temperature metalorganic vapor-phase epitaxial growth of InGaAs layers on InP substrates.” Journal of Crystal Growth. vol. 219, pp. 10-16, 2000.

25. Gao, Wei, Paul Berger, Matthew Ervin, Jagadeesh Pamulapati, Richard Lareau, and Stephen Schauer. “Liquid phase epitaxial growth of InGaAs on InP using rare-earth treated melts.” Journal of Applied Physics. vol. 80, pp. 7094-7103, 1996.

26. Raisanen, A., L. J. Brillson, R. S. Goldman, K. L. Kavanagh, and H. H. Wieder. “Optical detection of misfit dislocation-induced deep levels at InGaAs/GaAs heterojunctions.” Applied Physics Letters. vol. 64, pp.3572-3574, 1994.

27. Bacher, F. R. “Characterization of deep-level defects in $In_{1-x}Ga_xAs/InP$.” Journal of Applied Physics. vol. 64, pp. 706-712, 1987.

28. Watanabe, Kazuo, Fumiaki Hyuga, and Takumi Nittono. “Effect of annealing on the electrical properties of GaAs/InGaP/n^+InGaAs/GaAs epitaxial layers.” Journal of Applied Physics. vol. 84, pp.5614-5620, 1998.

29. Mangeney, J., L. Joulaud, J. Dcobert, J.-M. Lourtioz, J.L. Perossier, S. Cabaret, and P. Crozat. “Electrical properties of 1.55 μm sensitive ion-irradiated InGaAs with subpicosecond carrier lifetime.’ Electronics Letters. vol. 39, pp. 681-682, 2003.

30. Jouland, L., J. Mangeney, N. Chimot, P. Crozat, and G. Fishman. “Conduction mechanisms in ioin-irradiated InGaAs layers.” Journal of Applied Physics. vol. 97, 06315-1-7, 2005.

31. Dosluoglu, T. and R. Solanki. “The effect of InP buffer layer on the electron transport properties of epitaxial $In_xGa_{1-x}As$.” Journal of Applied Physics. vol. 69, pp. 7327-7329, 1991.

32. Wang, S.M., C. Karlsson, N. Rorsman, M. Bergh, D. Olsson, T.G. Andersson, and H. Zirath. “Molecular beam epitaxy growth and characterization of $In_xGa_{1-x}As$ ($0.57 \leq x \leq 1$)

on GaAs using InAlAs graded buffer." Journal of Crystal Growth. vol. 175/176, pp. 1016-1021, 1997.

33. Yeo, W., R. Dimitrov, W. J. Schaff, and L. F. Eastman. "Material properties of bulk InGaAs and InAlAs/InGaAs heterostructures grown on (111)B and (111)B misoriented by 1° towards $\langle 211 \rangle$ InP substrates." Applied Physics Letters. vol. 77, pp. 4292-4294, 2000.

34. Dhar, S., Shampa Paul, and V. N. Kulkarni. "Impurity reduction in $In_{0.53}Ga_{0.47}As$ layers grown by liquid phase epitaxy using Er-treated melts." Applied Physics Letters. vol. 76, pp. 1588-1590, 1999.

35. Gorelenok, A. T., A. V. Kamanin, and N. M. Shmidt. "Rare-Earth Elements in the Technology of III-V Compounds and Devices Based on These Compounds." Semiconductors. vol. 37. pp. 894-914, 2003.

REPORT DOCUMENTATION PAGE

Form Approved
OMB No. 074-0188

1. REPORT DATE *(DD-MM-YYYY)*	2. REPORT TYPE	3. DATES COVERED *(From – To)*
25-03-2010	Master's Thesis	March 2009 – March 2010

4. TITLE AND SUBTITLE
Optical and Electrical Characterization of Bulk Grown Indium-Gallium-Arsenide Alloys

5a. CONTRACT NUMBER

5b. GRANT NUMBER

5c. PROGRAM ELEMENT NUMBER

6. AUTHOR(S)
Bergstrom, Austin C., 2nd Lieutenant, USAF

5d. PROJECT NUMBER
175

5e. TASK NUMBER

5f. WORK UNIT NUMBER

7. PERFORMING ORGANIZATION NAMES(S) AND ADDRESS(S)
Air Force Institute of Technology
Graduate School of Engineering and Management (AFIT/EN)
2950 Hobson Way, Building 640
WPAFB OH 45433-8865

8. PERFORMING ORGANIZATION REPORT NUMBER
AFIT/GAP/ENP/10-M02

9. SPONSORING/MONITORING AGENCY NAME(S) AND ADDRESS(ES)
Dr. Donald Smith
AFOSR/RSE
825 N. Randolph St., Arlington, VA 22203

10. SPONSOR/MONITOR'S ACRONYM(S) AFOSR/RSE

11. SPONSOR/MONITOR'S REPORT NUMBER(S)

12. DISTRIBUTION/AVAILABILITY STATEMENT
APPROVED FOR PUBLIC RELEASE; DISTRIBUTION UNLIMITED.

13. SUPPLEMENTARY NOTES

14. ABSTRACT
Advances in crystal growth techniques have allowed increased quality in growth of bulk ternary $In_xGa_{1-x}As$. Here, the optical and electrical properties of samples grown through the vertical Bridgman (or multi-component zone melting growth) method have been investigated through photoluminescence spectroscopy and Hall effect measurements. Indium mole fractions varied from 0.75 for 1. Hall effect measurements at temperatures ranging from 10 to 300 K revealed moderate n-type doping with carrier concentrations ranging from 1.5 to 9.6×10^{16} cm^{-3} at 10 to 15 K. Carriers from deep donor levels became appreciable between 50 and 100 K. Hall mobility increased with rising indium content, and mobility values at 15 K ranged from 1.5×10^{4} $cm^2/(V\cdot s)$ for $In_{0.75}Ga_{0.25}As$ to 3.5×10^{4} $cm^2/(V\cdot s)$ for InAs. Mobility variation with temperature showed ionized impurity scattering to be dominant at low temperatures with optical phonon scattering becoming dominant near 100 K. Laser excitation power dependent photoluminescence measurements were performed at 12 K, and temperature dependent photoluminescence measurements were performed at temperatures ranging from approximately 12 to 140 K. Photoluminescence measurements showed band-to-band and donor-acceptor pair transitions. 12 K band-to-band photoluminescence peak positions loosely followed predicted band gaps, and position dependent photoluminescence measurements revealed varying degrees of uniformity across the samples studied.

15. SUBJECT TERMS
Indium Gallium Arsenide, Bulk Ternary Alloy, Electrical Characterization, Optical Characterization, Hall Effect, Photoluminescence, Carrier Concentration, Mobility, Semiconductor

16. SECURITY CLASSIFICATION OF:			17. LIMITATION OF ABSTRACT	18. NUMBER OF PAGES	19a. NAME OF RESPONSIBLE PERSON
a. REPORT	b. ABSTRACT	c. THIS PAGE			Dr. Yung Kee Yeo, ENP
U	U	U	UU	91	19b. TELEPHONE NUMBER *(Include area code)* (937) 255-3636, x4532; email: yung.yeo@afit.edu

Standard Form 298 (Rev. 8-98)
Prescribed by ANSI Std. Z39-18